COMPLEMENT

Copyright © 2023 The Authors, some rights reserved; exclusive licensee American Association for the Advancement of Science. No claim to original U.S. Government Works

Lung epithelial cell–derived C3 protects against pneumonia-induced lung injury

Sanjaya K. Sahu[1]†, Ayşe N. Ozantürk[1]†, Devesha H. Kulkarni[2], Lina Ma[1], Ruteja A. Barve[3], Linus Dannull[1], Angel Lu[1], Marick Starick[1], Ja'Nia McPhatter[1], Lorena Garnica[1], Maxwell Sanfillipo-Burchman[4], Jeremy Kunen[1], Xiaobo Wu[5], Andrew E. Gelman[6], Steven L. Brody[1], John P. Atkinson[5], Hrishikesh S. Kulkarni[1]*

The complement component C3 is a fundamental plasma protein for host defense, produced largely by the liver. However, recent work has demonstrated the critical importance of tissue-specific C3 expression in cell survival. Here, we analyzed the effects of local versus peripheral sources of C3 expression in a model of acute bacterial pneumonia induced by *Pseudomonas aeruginosa*. Whereas mice with global C3 deficiency had severe pneumonia-induced lung injury, those deficient only in liver-derived C3 remained protected, comparable to wild-type mice. Human lung transcriptome analysis showed that secretory epithelial cells, such as club cells, express high levels of C3 mRNA. Mice with tamoxifen-induced C3 gene ablation from club cells in the lung had worse pulmonary injury compared with similarly treated controls, despite maintaining normal circulating C3 levels. Last, in both the mouse pneumonia model and cultured primary human airway epithelial cells, we showed that stress-induced death associated with C3 deficiency parallels that seen in Factor B deficiency rather than C3a receptor deficiency. Moreover, C3-mediated reduction in epithelial cell death requires alternative pathway component Factor B. Thus, our findings suggest that a pathway reliant on locally derived C3 and Factor B protects the lung mucosal barrier.

INTRODUCTION

Pathogens infect and injure mucosal surfaces, resulting in a cascade of events including inflammation, tissue damage, and systemic dissemination (*1*, *2*). In the lung, this process results in severe pneumonia, a leading cause of human death even before the severe acute respiratory syndrome coronavirus 2 (SARS-CoV-2) pandemic (*3*, *4*). The outcome of pneumonia is determined by a balance between immune resistance and tissue resilience (*1*, *5*). Immune resistance is the host's ability to eradicate pathogens, whereas tissue resilience is the ability of the lung to withstand the deleterious consequences of infection and inflammation (*1*, *5*). The complement system is a family of immune proteins that facilitate immune resistance by attacking microbes to decrease pathogen burden (*6*, *7*). The cascade can be activated by multiple arms such as the classical, lectin, or alternative pathway, and each of them plays important roles in host defense (*8*, *9*). Genetic and acquired deficiencies of complement consequently lead to recurrent bacterial infections in both children and adults (*10*, *11*). Recently, there has been an increasing appreciation of how the system functions to promote tissue resilience in the setting of acute infections (*12*, *13*).

A majority of complement proteins are liver derived (*14*). One such protein, C3, is a central component of the complement system, because multiple pathways converge on its activation to C3a and C3b, thereby amplifying the cascade (*15*). C3a promotes host defense by binding to its cognate receptor, C3aR, whereas C3b binds to Factor B (FB) and modulates outcomes of bacterial infection via the alternative pathway (*9*). The normal plasma concentration of C3 is 1 to 2 g/liter in humans, making it one of the most common proteins in the circulation after other liver-derived proteins such as albumin and α-2-macroglobulin (*16*). Thus, the protective effects of C3 have largely been attributed to it being sourced from the liver and present in a high concentration in the circulation. However, we and others have previously demonstrated that C3 is also produced outside the liver by multiple immune and nonimmune cell populations (*17*–*22*). This observation has implications, especially for organs that constantly interact with pathogens and environmental toxins, such as the lung (*6*, *23*). For example, we have demonstrated that C3 synthesized and internalized by lung epithelial cells protects against stress-induced cell death (*18*, *24*). Others have demonstrated that chronic C3 up-regulation in lung epithelial cells can perpetuate inflammation in SARS-CoV-2 infection (*21*).

It is unknown whether cell-intrinsic C3 production is relevant in vivo. It is also unclear whether the protective effects of C3 are purely a result of enhancing immune resistance via its bactericidal activity or whether it also contributes to tissue resilience by reducing acute lung injury (ALI). To address these questions, we used a model of acute *Pseudomonas aeruginosa* (*Pa*) pneumonia in mice globally deficient in C3 and report that C3 not only promotes immune resistance but also enhances tissue resilience in vivo by mitigating ALI. Using publicly available human lung datasets and a C3 reporter mouse model, we established that multiple cell types in the lung produce and up-regulate C3 in the setting of *Pa* infection. Building

[1]Division of Pulmonary and Critical Care Medicine, John T. Milliken Department of Medicine, Washington University School of Medicine, St. Louis, MO, USA. [2]Division of Gastroenterology, John T. Milliken Department of Medicine, Washington University School of Medicine, St. Louis, MO, USA. [3]Department of Genetics, Washington University School of Medicine, St. Louis, MO, USA. [4]Division of Allergy and Pulmonary Medicine, Department of Pediatrics, Washington University School of Medicine, St. Louis, MO, USA. [5]Division of Rheumatology, John T. Milliken Department of Medicine, Washington University School of Medicine, St. Louis, MO, USA. [6]Department of Surgery, Washington University School of Medicine, St. Louis, MO, USA.
*Corresponding author. Email: hkulkarn@wustl.edu
†These authors contributed equally to this work

Downloaded from https://www.science.org at University of Massachusetts Worcester on February 08, 2023

on these findings, we generated mouse strains and showed that lung epithelial cell–derived C3 is functioning locally, independent of circulating (i.e., liver derived) C3, and is necessary for reducing *Pa*-induced ALI. Using both human in vitro and mouse in vivo infection models, we showed that cell-intrinsic FB, a component of the alternative pathway and a ligand for C3, is a key component of tissue resilience, enhancing the ability of the lung to withstand the deleterious consequences of infection and inflammation. Our findings potentially refine the approach for therapeutically targeting the complement system in the lung, with the goal of mitigating bacterial pneumonia severity.

RESULTS

C3 protects against severe bacterial pneumonia

C3-deficient mice had histological evidence of increased lung injury when compared with wild-type (WT) mice 24 hours after *Pa* infection (Fig. 1A). Physiological function was impaired, as demonstrated by reduced dynamic compliance (Fig. 1B) and higher airway resistance compared with WT (fig. S1A), both measured by whole-body plethysmography 24 hours after infection. Lung wet-dry ratios showed that C3-deficient mice had increased alveolar-capillary barrier permeability (fig. S1B). We next analyzed inflammatory gene expression. C3-deficient mice had an exaggerated inflammatory response, as determined by increased lung *Ccl2* and *Il1b* expression (Fig. 1C), the proportion of bronchoalveolar lavage (BAL) Ly6C^{hi} monocytes (fig. S1C), and BAL C-C motif chemokine ligand 2 (CCL2) and interleukin-1β (IL-1β) levels (fig. S1, D and E). The BAL levels of IL-6 and tumor necrosis factor–α (TNF-α) showed a trend toward significance in C3-deficient mice compared with WT mice (fig. S1, F and G). Infected C3-deficient mice had lower expression of epithelial cell genes *Scgb1a1* (representing secretory airway epithelial cells) and *Sftpc* (representing alveolar epithelial cells) compared with infected WT, suggesting that C3 protects against epithelial cell loss (Fig. 1C). However, C3-deficient mice also had higher lung (Fig. 1D) and splenic bacterial counts (Fig. 1E) at 24 hours after *Pa* infection.

One explanation for increased lung injury in C3-deficient mice is damage induced by actively proliferating bacteria. To this end, heat-killed *Pa* (HK*Pa*) was administered intratracheally into both C3-deficient and WT mice, and lungs and BAL were harvested 24 hours later. Compared with WT, C3-deficient mice still retained more histologic evidence of lung injury (Fig. 1, F and G), characterized by an increase in alveolar (fig. S1H) and interstitial neutrophilia (fig. S1I) and septal thickening (fig. SJ). HK*Pa*-treated C3-deficient mice also had increased alveolar-capillary barrier permeability (Fig. 1H), increased total BAL cell count (Fig. 1I), and increased lung *Ccl2* and *Il1b* expression (Fig. 1J). C3-deficient mice treated with HK*Pa* had a lower proportion of lung epithelial cells (Fig. 1K) and lower expression of *Scgb1a1* and *Sftpc* compared with WT mice treated with HK*Pa* (Fig. 1L). These observations suggest increased epithelial cell loss after infection in the setting of C3 deficiency, independent of bacterial load.

C3 in the lungs is sourced locally

C3 increases in the BAL of both mice and humans after lung injury (*25*). To determine whether this C3 is functional, we adapted our previously established in vitro complement assay, which considers both the activation [using lipopolysaccharide (LPS)] and the function of the complement cascade (*26*–*28*). Functional complement activity in the sera of WT mice was intact before and 24 hours post *Pa* infection (Fig. 2A). In comparison with sera, functional complement activity in the BAL of WT mice was up-regulated several thousandfold at 24 hours after *Pa* infection compared with BAL levels in uninfected mice (Fig. 2B). These observations would suggest that functional complement activity is rapidly induced in an organ with low baseline activity in the first 24 hours after infection. To determine the contribution of circulating C3 to that in the BAL, we administered normal mouse serum (NMS; obtained from WT mice) intraperitoneally to C3-deficient mice after intratracheal instillation of *Pa* (to induce injury) or phosphate-buffered saline (PBS; control). Either NMS was given immediately after the *Pa* infection and the mice were followed for 24 hours before euthanasia, or it was given 1 hour before euthanasia, by which time the *Pa*-induced injury had already occurred. C3 was detected in the BAL at 24 hours after NMS administration only in the C3-deficient mice administered with NMS, which had alveolar-capillary barrier disruption in the setting of *Pa* pneumonia, not in those who had only received intratracheal PBS (Fig. 2C). However, C3 was not detected in the BAL at 1 hour after NMS administration even if the lungs had been injured by *Pa*, despite being detected in the circulation. These observations suggest that after disruption of the alveolar-capillary barrier, circulating C3 entry into the alveolar space is delayed relative to local C3 secretion. Splenic bacterial dissemination and weight loss were lower in mice administered with NMS compared with those given C3-deficient serum (fig. S2, A and B). However, epithelial cell death, as measured by the decrease in the club cell ratio in vivo, was similar between the two groups (fig. S2C).

To quantify C3 expression and production by different cell types, we used C3 reporter mice with an IRES (internal ribosome entry side)–tdTomato cassette after the stop signal in the endogenous murine C3 locus, with exons 37 to 41 sequence flanked by loxP sites, enabling its conditional deletion upon the action of a *Cre* recombinase (*17*). Given that the liver is the major source of circulating C3, we bred these mice to generate an in vivo model of C3 deficiency restricted to the liver (*C3*$^{f/f}$; *Alb-Cre*$^{+/-}$; Fig. 2D). We confirmed that these mice had no expression of C3 in the liver (Fig. 2E) and undetectable levels of circulating C3 compared with littermate controls and WT mice both before and after *Pa* infection (Fig. 2F). Although C3 was undetectable in the BAL before infection in the *C3*$^{f/f}$; *Alb-Cre*$^{+/-}$ mice, it increased at 24 hours after *Pa* infection, suggesting locally sourced C3 (Fig. 2G). This increase was lower than what was observed in littermate controls.

Although there was no functional complement activity in the circulation of the *C3*$^{f/f}$; *Alb-Cre*$^{+/-}$ mice as compared with their littermate controls before infection (Fig. 2H), complement from BAL in *C3*$^{f/f}$; *Alb-Cre*$^{+/-}$ mice was still functional (Fig. 2I). After infection, there was no increase in functional complement activity in the circulation of *C3*$^{f/f}$; *Alb-Cre*$^{+/-}$ mice as compared with preinfection levels (Fig. 2H). In comparison, functional complement activity in the BAL increased at 24 hours after infection in *C3*$^{f/f}$; *Alb-Cre*$^{+/-}$ mice (Fig. 2I). Together, these observations suggest that although circulating C3 is functional in the lung in the setting of an acute infection, extrahepatic sources of C3 also contribute to C3 function in the lung.

Given the lack of both detectable circulating C3 in the *C3*$^{f/f}$; *Alb-Cre*$^{+/-}$ mice and any functional complement activity in the serum,

Downloaded from https://www.science.org at University of Massachusetts Worcester on February 08, 2023

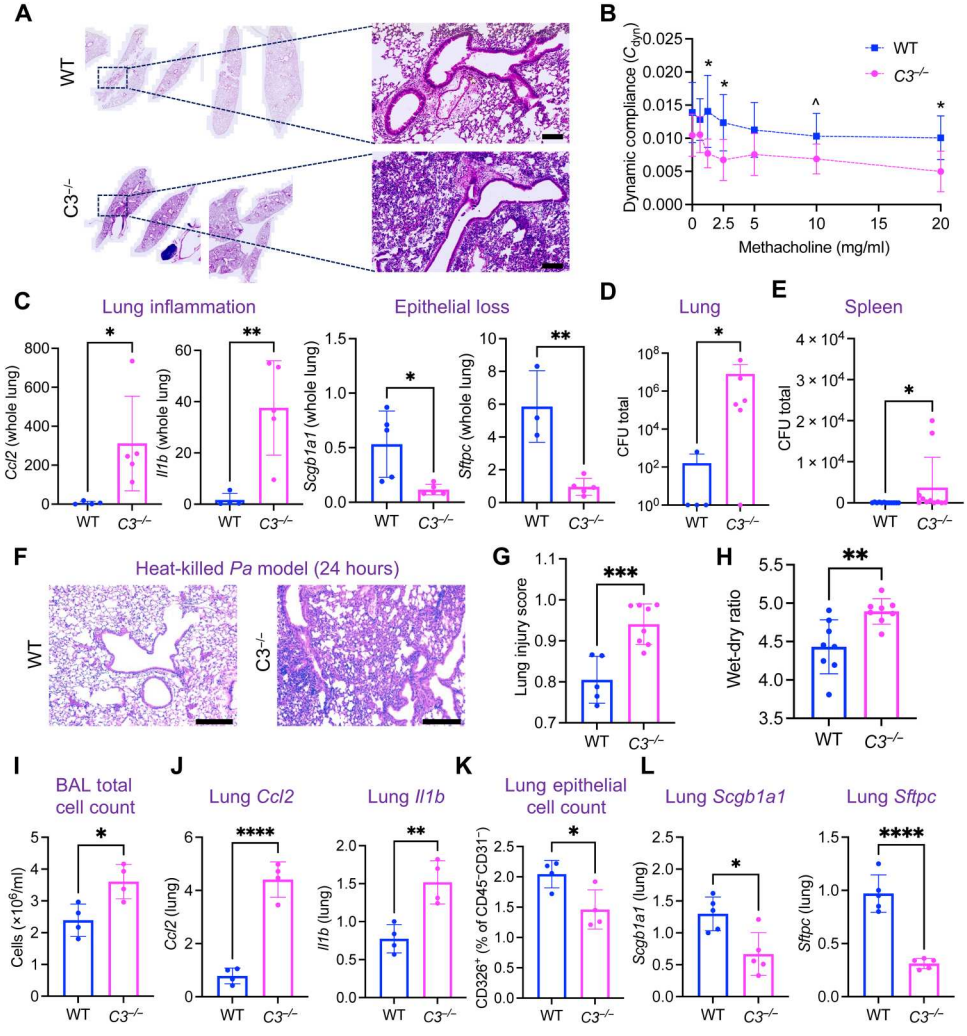

Fig. 1. C3 protects against severe bacterial pneumonia. (**A** to **E**) Global C3-deficient ($C3^{-/-}$) and WT B6 mice were euthanized 24 hours after infection with *Pa*. (A) Representative images from $n = 5$ mice per group; an area of magnification shows both the airways and alveolar space [scale bars (black), 100 μm]. (B) To assess physiological dysfunction, we performed small animal whole-body plethysmography using increasing concentrations of methacholine from 0.625 to 20 mg/ml (*x* axis) on $C3^{-/-}$ ($n = 4$) and WT ($n = 7$) mice. Dynamic compliance (in milliliters per centimeter of H_2O) is represented on the *y* axis. (C) Quantitative RT-PCR (qRT-PCR) measurements for *Ccl2*, *Il1b*, *Scgb1a1* (an airway club cell marker), and *Sftpc* (an alveolar type II cell marker), all normalized to *Gapdh*. (D and E) CFU in the harvested (D) lungs and (E) spleens. *X* axis is on a logarithmic scale. (**F** to **L**) $C3^{-/-}$ and WT mice were euthanized 24 hours after infection with HK*Pa*. (F) Representative histology images [$n = 5$ to 8 per group; scale bars (black), 250 μm]. Differences in (G) lung injury scores, (H) lung wet-dry ratios, (I) BAL cell count, (J) qRT-PCR for *Ccl2* and *Il1b*, (K) proportion of epithelial cells (gated as $CD45^-CD31^-CD326^+$) from digested mouse lungs, and (L) qRT-PCR for *Scgb1a1* and *Sftpc*. (J) and (L) are normalized to *Hprt1*. Distribution of data is represented as scatterplots showing individual data points, and bars represent means ± SD. ^$P < 0.1$, *$P < 0.05$, **$P < 0.01$, ***$P < 0.001$, and ****$P < 0.0001$ using unpaired two-tailed *t* test.

we hypothesized that functional complement activity in the BAL of $C3^{f/f}$; *Alb-Cre*$^{+/-}$ mice was generated from the lung. The presence of a functional extrahepatic source of C3 was corroborated by lower splenic dissemination of bacteria in $C3^{f/f}$; *Alb-Cre*$^{+/-}$ mice as compared with global C3-deficient mice (Fig. 2J). Moreover, there was no difference in lung wet-dry ratio (Fig. 2K), BAL cell count (Fig. 2L), or histological evidence of injury (fig. S2D) in mice deficient in liver-derived C3 as compared with littermate controls at 24 hours after *Pa* infection, although all these features of lung injury were increased in global C3-deficient mice. These observations suggest that lung epithelial cell–derived C3 plays a key role in mitigating bacterial pneumonia–induced lung injury. No differences were observed in BAL cytokine levels in mice deficient in liver-derived C3 as compared with their littermate controls at 24 hours after *Pa* infection (fig. S2, E to H).

Nonimmune cells contribute to C3 in the lung

To evaluate sources of C3 in the normal human lung, we analyzed public single-cell RNA sequencing (RNA-seq) datasets from the Lung Gene Expression Atlas (LGEA) and LungMAP (*29*–*32*). Our analysis showed that although most cells express C3 transcripts, major sources of C3 in the lungs are epithelial cells, fibroblasts, and, to a lesser extent, monocytes/macrophages (Fig. 3A and fig. S3A). To identify cell-intrinsic production of C3 in the lungs in

Downloaded from https://www.science.org at University of Massachusetts Worcester on February 08, 2023

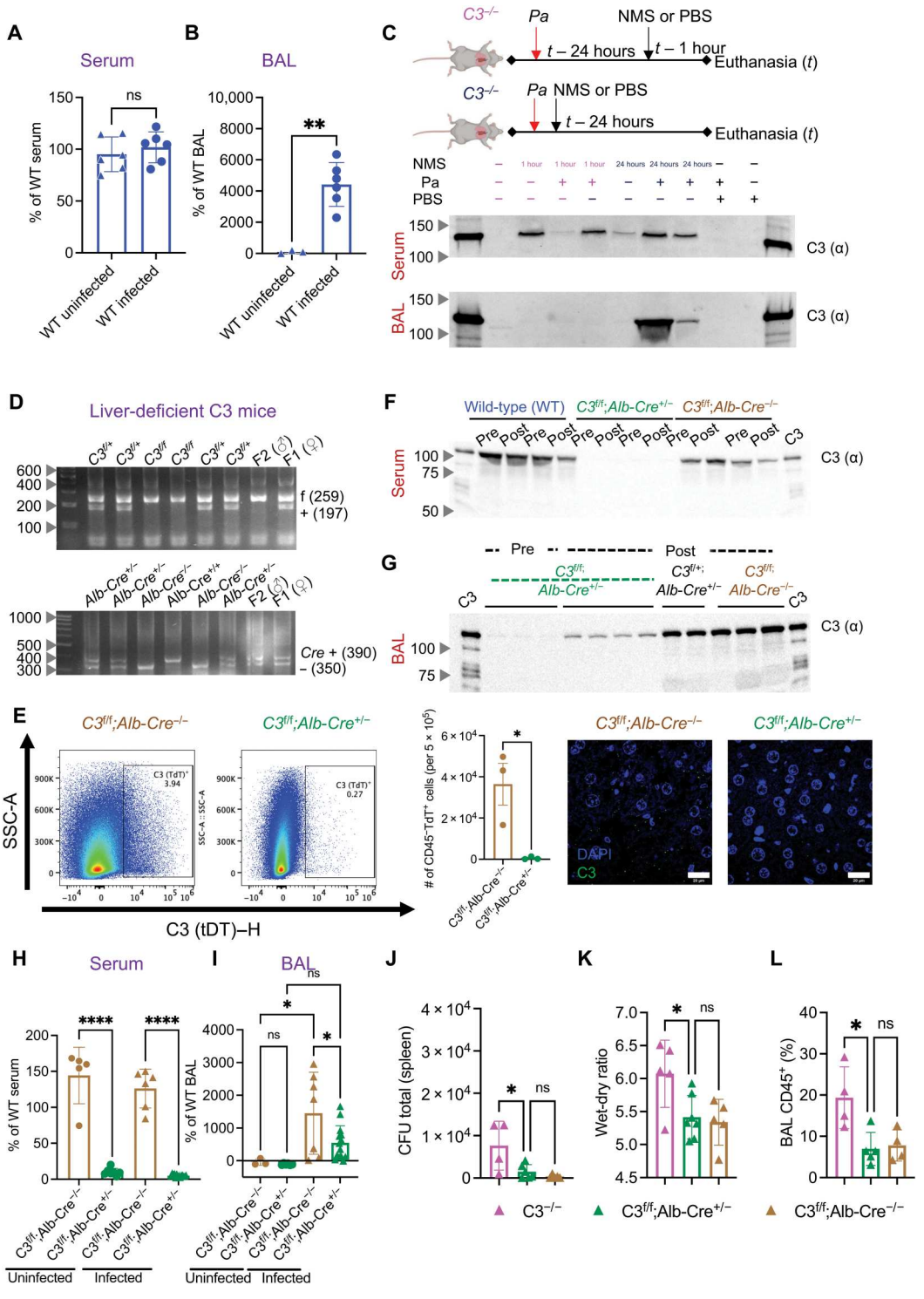

Fig. 2. C3 in the lungs is sourced locally. LPS-induced complement activation in (**A**) mouse serum and (**B**) BAL assessed in both uninfected and infected WT mice. Results expressed as percentage activity of concurrently run uninfected WT B6 mouse sera and BAL, respectively. (**C**) Infected *C3*$^{-/-}$ mice were administered with NMS (10 μl/g of body weight) or PBS intraperitoneally either 1 or 24 hours before euthanasia (i.e., at the time of infection). (**D**) PCR products from genomic DNA separated by agarose gel electrophoresis used to identify mice deficient in liver-derived C3 and their littermate controls. (**E**) Livers from *C3*$^{f/f}$; *Alb-Cre*$^{+/-}$ and *C3*$^{f/f}$; *Alb-Cre*$^{-/-}$ mice were analyzed using flow cytometry using negative selection (gated on CD45^{-} to exclude immune cells). C3 expression was assessed using tdTomato reporter (n = 3 mice per group). Representative immunofluorescence from livers of each of the groups showing C3 (in green) and DAPI (blue) [scale bars (white), 20 μm]. Immunoblots of reduced (**F**) sera and (**G**) BAL from mice, obtained before and after *Pa* infection. To assess functional activity in liver-derived C3-deficient mice, we assessed LPS-induced complement activation in (**H**) mouse serum and (**I**) BAL. Comparison of (**J**) spleen CFU (x axis is on a logarithmic scale), (**K**) lung wet-dry ratios, and (**L**) BAL immune cell counts after infection. Distribution of data is represented as scatterplots showing individual data points, and bars represent means ± SD. *P < 0.05, **P < 0.01, and ****P < 0.0001 using unpaired two-tailed t test and ordinary one-way ANOVA with Šidák's multiple comparisons testing for more than two groups.

the absence of circulating C3, we profiled C3-producing nonimmune cells in the *Pa*-infected liver-derived C3-deficient reporter mice (*C3*$^{f/f}$; *Alb-Cre*$^{+/-}$) described earlier. In these mice, C3 increased by about threefold in airway epithelial cells and type 1 alveolar epithelial cells and increased by nearly fourfold from baseline in type 2 alveolar epithelial cells, fibroblasts, and endothelial cells at 24 hours after *Pa* infection (Fig. 3B and fig. S3B). We have previously shown that lung epithelial cells expressing SCGB1A1 (i.e., CCSP) are a major source of C3 in humans, especially in diseases associated with recurrent infections such as cystic fibrosis (*18*), and we were interested in how C3 from cells at the mucosal barrier surface affects the host response to pneumonia. Hence, we generated *C3*$^{f/f}$; *Scgb1a1*-CreERT2$^{+/-}$ mice to specifically delete C3 produced by lung epithelial cells (club cell–deficient C3 mice), which

Downloaded from https://www.science.org at University of Massachusetts Worcester on February 08, 2023

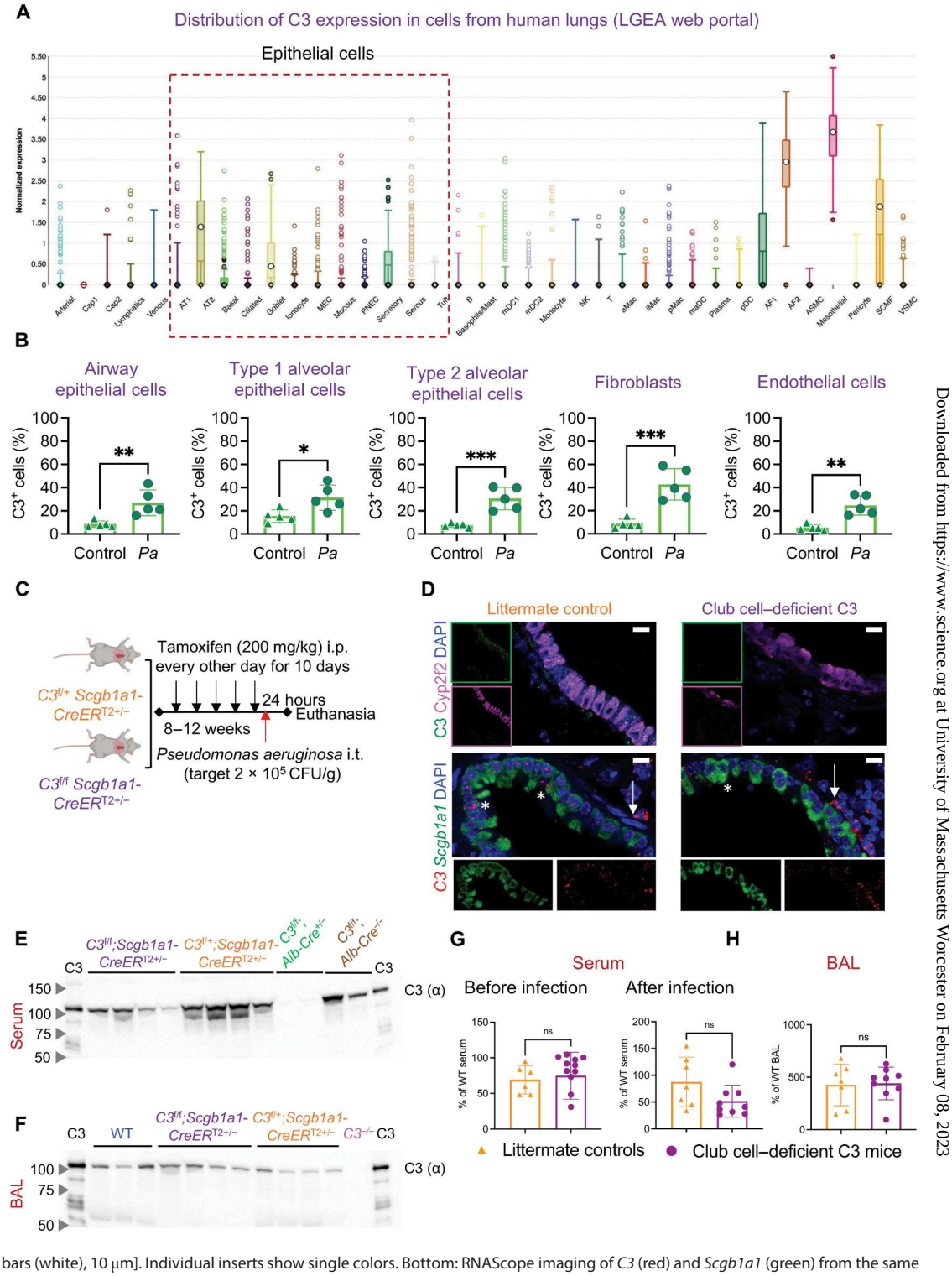

Fig. 3. Nonimmune cells contribute to C3 in the lung. (**A**) Human lung expression of C3 (ENSG00000125730) using the LungMAP Single Cell Reference (v1) in the LGEA web portal (LungMAP Phase 2). AF1, alveolar matrix fibroblast 1; AF2, alveolar matrix fibroblast 2; aMac, alveolar macrophages; ASMC, airway smooth muscle cells; AT1, type 1 alveolar epithelial cells, AT2, type 2 alveolar epithelial cells; Cap1, capillary 1 cells; Cap2, capillary 2 cells; iMac, interstitial macrophages; maDC, mature human dendritic cell; mDC1, myeloid dendritic cell subset 1; mDC2, myeloid type 2 dendritic cell; MEC, myoepithelial cells; NK, natural killer cells; pDC, plasmacytoid dendritic cells; pMac, proliferative macrophages; PNEC, pulmonary neuroendocrine cells; SCMF, secondary crest myofibroblasts; VSMC, vascular smooth muscle cells; i.p., intraperitoneally; i.t., intratracheally. (**B**) Changes in C3 expression on flow cytometry in cells obtained from the lungs of noninfected (Control) and infected (*Pa*) mice deficient in liver-derived C3 ($C3^{f/f}$; *Alb-Cre*$^{+/-}$, $n = 5$ per group). Airway epithelial cells, $CD45^-CD31^-EpCAM^+$ $PDPN^+$; type 1 alveolar epithelial cells, $CD45^-CD31\text{-}EpCAM^+$ $PDPN^-CD104^+$; type 2 alveolar epithelial cells, $CD45^-CD31\text{-}EpCAM^+$ $PDPN^-$ $CD104^-$; fibroblasts, $CD45^-CD31^-$ $EpCAM^-Sca\text{-}1^+$; endothelial cells, $CD45^-CD31^+$. (**C**) Schematic for tamoxifen induction of *Cre* recombinase followed by infection. (**D**) Top: Confocal microscopy imaging of C3 (green; FITC equivalent 488-nm laser) and Cyp2f2 (pink; Cy5 equivalent 640-nm laser) in the lungs of $C3^{f/f}$; *Scgb1a1*-$CreERT2^{+/-}$ mice as compared with controls that have normal C3 and Cyp2f2 expression. Cyp2f2 was used as the club cell marker instead of Scgb1a1, because antibodies to both C3 and Scgb1a1 are of the same species [table S2; representative of $n = 4$ per group; scale bars (white), 10 μm]. Individual inserts show single colors. Bottom: RNAScope imaging of *C3* (red) and *Scgb1a1* (green) from the same genotypes. The asterisk represents C3 in the club cells, which is reduced in the *Scgb1a1*-$CreERT2^{+/-}$ mice. The arrow represents cells other than the epithelial cells (e.g., immune cells) that express C3. Scale bars (white), 10 μm. Immunoblots of reduced (**E**) sera and (**F**) BAL from lung-derived C3-deficient mice and littermate controls. Mice deficient in liver-derived C3 and their littermate controls have been used as a comparison for the serum immunoblots, and $C3^{-/-}$ mice have been used to compare BAL. (**G**) LPS-induced complement activation in mouse serum. (**H**) The same assay performed on BAL after infection. Distribution of data is represented as scatterplots showing individual data points, and bars represent means ± SD. **P* < 0.05, ***P* < 0.01, and ****P* < 0.001 using unpaired two-tailed *t* test.

Downloaded from https://www.science.org at University of Massachusetts Worcester on February 08, 2023

are hereafter referred to as mice deficient in lung epithelial cell–derived C3 (Fig. 3C and fig. S3C). Successful deletion of C3 from club cells was confirmed using immunofluorescence for C3 and Cyp2f2, a club cell marker (Fig. 3D) (*33*–*35*). These mice deficient in lung epithelial cell–derived C3 had similar levels of C3 in their circulation and BAL as their littermate controls (Fig. 3, E and F). They also had similar serum and BAL functional complement activity compared with their littermate controls (Fig. 3, G and H).

Epithelial (club) cell–derived C3 protects against severe bacterial pneumonia

C3$^{f/f}$; *Scgb1a1*-CreERT2$^{+/-}$ mice had more ALI after *Pa* infection than their littermate controls, as represented by measures of alveolar-capillary barrier disruption (Fig. 4, A and B). They also had more severe histology (Fig. 4C) and an exaggerated inflammatory response as seen by increased BAL cytokine levels of IL-1β, IL-6, keratinocyte chemoattractant (KC), and TNF-α (Fig. 4, D to G). In addition, mice deficient in lung epithelial cell–derived C3 demonstrated increased epithelial cell injury compared with littermate controls, indicated by a marked increase in BAL receptor for advanced glycation end products (RAGE) levels (Fig. 4H), as well as increased epithelial cell death, as represented in the fluid phase by an increase in BAL cytokeratin-18 (CK-18) levels (Fig. 4I) and in situ by a decreased club cell ratio on lung histopathology (Fig. 4J) (*36*–*38*). A similar pattern of lung injury was seen in the intratracheal HK*Pa* model, where mice deficient in lung epithelial cell–derived C3 had increased measures of alveolar-capillary barrier disruption (Fig. 4K), epithelial cell loss (Fig. 4L), and a decreased club cell ratio in situ (Fig. 4M and fig. S3D). These findings suggest that lung epithelial cell–derived C3 reduces *Pa*-induced lung injury despite adequate circulating (i.e., liver-derived) C3 levels.

Complement Factor B protects against stress-induced epithelial injury in vivo

Upon activation, C3 is cleaved to form C3a, which binds to the C3a receptor (C3aR), and C3b fragments, which not only can opsonize targets but also bind FB to form a C3 convertase (C3bBb) and amplify the alternative pathway of the complement cascade (*39*). To assess which of these putative targets may be facilitating the protective effects of C3 in the lung, we infected global C3aR-deficient (*C3aR*$^{-/-}$) and FB-deficient (*Cfb*$^{-/-}$) mice. C3aR-deficient mice were relatively protected from *Pa*-induced ALI and had a pattern of injury that was similar to that of the WT mice (Figs. 5A and 1A). In comparison, FB-deficient mice had more severe injury (Fig. 5A). Increased lung stiffness (as demonstrated by decreased dynamic compliance) was observed at 24 hours after infection in FB-deficient mice compared with WT mice at higher doses of methacholine (fig. S4A). In comparison, there was no significant difference in lung stiffness in C3aR-deficient mice compared with WT mice at higher doses of methacholine (fig. S4A). There was increased alveolar-capillary barrier disruption after infection, as evidenced by an increased lung wet-dry ratio in FB-deficient mice compared with WT and C3aR-deficient mice (Fig. 5B). FB-deficient mice had increased inflammation after infection, as measured by *Il1b* (Fig. 5C) and *Ccl2* (fig. S4B) expression, and an increased number of Ly6C^{hi} monocytes in the lungs compared with WT mice (fig. S4C). FB-deficient mice also had increased epithelial cell loss, measured by lung *Scgb1a1* (Fig. 5D), *Sftpc* (fig. S4D), and *Cdh1* (fig. S4E) expression, and increased epithelial cell death compared with WT mice as measured by BAL CK-18 levels (fig. S4F) and confirmed using amine dye exclusion on flow cytometry (fig. S4G).

A similar pattern of increased lung injury in the setting of FB deficiency was observed after HK*Pa* administration. FB-deficient mice given HK*Pa* had increased lung injury on histology (Fig. 5, E and F), as well as an increased wet-dry ratio as compared with WT mice (Fig. 5G). These mice also had significantly higher expression of *Il1b* (Fig. 5H) and *Ccl2* (fig. S4H) in their lungs, which paralleled our findings in C3 deficiency. FB-deficient mice had decreased *Scgb1a1* (Fig. 5I), *Sftpc* (fig. S4I), and *Cdh1* (fig. S4J) expression in their lungs after HK*Pa* administration as compared with WT mice, suggesting epithelial cell loss in the setting of injury. To determine whether epithelial cell death in C3 and FB deficiency precedes immune cell infiltration, we performed flow cytometric analysis on the lungs at earlier time points. Epithelial cell death was increased in C3-deficient and FB-deficient mice at the 16-hour time point compared with WT mice, before differences in immune cell infiltration (Fig. 5, J to L, and fig. S4, K and L). This observation supports the hypothesis that C3 and FB protect lung epithelial cells during an acute pneumonic insult in vivo.

Intracellular complement Factor B is upregulated in airway epithelial cells during *Pa* infection

Given that *Pa* induces bronchopneumonia, we sought to model these interactions among C3, C3aR, and FB in primary human airway epithelial cells. We previously reported that C3 increases in primary human tracheobronchial epithelial cells (hTECs) with stress (*18*). In hTECs infected with *Pa*, C3 and FB biosynthesis, as well as secretion, increased after infection, but levels of C3aR remained unchanged (Fig. 6A). This increase in FB was primarily observed in cytoplasmic and membrane subcellular fractions (Fig. 6B). C3 colocalized with intracellular FB stores during acute *Pa* infection, but colocalization with the C3aR was not observed (Fig. 6C). The increase in intracellular FB stores in primary hTECs paralleled what was observed in the lungs of mice deficient in club cell–derived C3 in the setting of *Pa*-induced injury. Specifically, we saw an increase in intracellular FB stores in vivo at 24 hours after HK*Pa* infection in the club cells of these mice (Fig. 6D). Hence, we subsequently characterized the consequences of FB deficiency in vitro in human lung epithelial cells using CRISPR-Cas9 deletion (fig. S5A) compared with C3aR deficiency (fig. S5B). We first used a model of oxidative stress based on our prior work (*18*) to avoid any effects of bacterial proliferation or toxin production. In an in vitro model of H_2O_2-induced stress, FB deficiency was associated with increased cell death compared with parent clones over time (fig. S5C). By comparison, C3aR deficiency was protective against H_2O_2-induced cell death, especially within the first 24 hours (fig. S5D).

Complement Factor B protects against stress-induced epithelial injury in vitro

RNA-seq analysis of *Pa*-infected FB-deficient cells and their infected FB-sufficient parental clones (Fig. 7A) using COMPBIO (COmprehensive Multi-omics Platform for Biological InterpretatiOn), an ontology-free analysis approach (Fig. 7B), identified cell death as a major (central) theme. "Cell death" shared common biology with two other themes: "autocrine-paracrine signaling" and "extracellular matrix (ECM) proteoglycans" (Fig. 7C), all of which were

Downloaded from https://www.science.org at University of Massachusetts Worcester on February 08, 2023

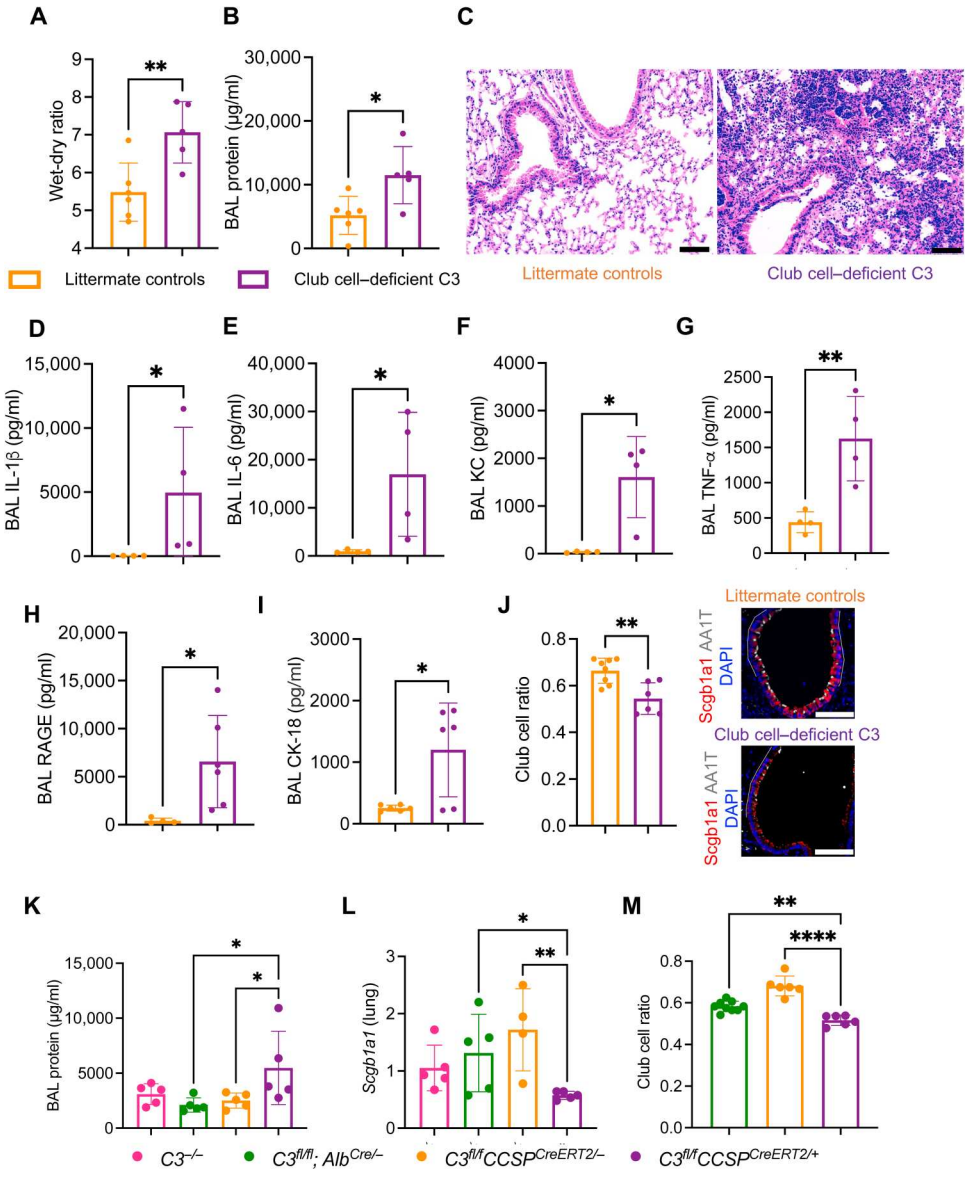

Fig. 4. Epithelial cell–derived C3 protects against severe bacterial pneumonia. Mice deficient in epithelial club cell–derived C3 (lung epithelial cell–derived C3, *C3*$^{f/f}$; *Scgb1a1*-CreERT2$^{+/-}$ mice) had worse alveolar-capillary barrier dysfunction at 24 hours after *Pa* infection compared with their littermate controls, as represented by (**A**) lung wet-dry ratio and (**B**) BAL protein. (**C**) Representative lung histology images of mice deficient in lung epithelial cell–derived C3 and their littermates at 24 hours after infection [scale bars (black), 75 μm; $n = 5$ per group]. (**D** to **G**) Comparison of lung inflammation in mice deficient in lung epithelial cell–derived C3 versus their littermates using cytokines such as IL-1β, IL-6, KC (CXCL1), and TNF-α in the BAL. (**H**) Comparison of epithelial cell injury using the levels of RAGE in the BAL. (**I**) Comparison of epithelial cell death using the levels of CK-18 in the BAL. (**J**) Comparison of club cell ratio, obtained by dividing the club cell numbers (Scgb1a1^{+}) in the lung histologic sections by the sum of the club cells (Scgb1a1^{+}) + ciliated cells [acetylated α-tubulin positive (AA1T^{+})]. Representative images are shown for comparing club cells (Scgb1a1, red) and ciliated cells (AA1T, gray) in *C3*$^{f/f}$; *Scgb1a1*-CreERT2$^{+/}$ and littermate control mice [DAPI, blue; scale bars (white), 75 μm]. *C3*$^{f/f}$; *Scgb1a1*-CreERT2$^{+/-}$ mice, their controls, and *C3*$^{f/f}$; *Alb*-Cre were euthanized 24 hours after infection with HK*Pa*. Differences in (**K**) BAL protein levels and (**L**) qRT-PCR for *Scgb1a1* (normalized to *Hprt1*) are shown. (**M**) A direct in situ comparison of epithelial cell death after HK*Pa* using the club cell ratio. Representative images in fig. S3D. Distribution of data is represented as scatterplots showing individual data points, and bars represent means ± SD. *$P < 0.05$, **$P < 0.01$, and **** $P < 0.0001$ using unpaired two-tailed *t* test or Mann-Whitney test and ordinary one-way ANOVA with Šidák's multiple comparisons testing for more than two groups.

present in the top five enriched themes in the analysis between FB-deficient cells and their parent clones (Fig. 7B and fig. S6). These three themes shared a common signature consisting of 18 genes, and their contributions are highlighted in the pseudo heatmap (Fig. 7C). FB deficiency was associated with increased programmed cell death, evident by increased cleaved caspase-8, caspase-3, and cleaved poly(adenosine diphosphate–ribose) polymerase (PARP) levels after *Pa* infection (Fig. 7D), and was paralleled by similar changes in the setting of oxidative stress (Fig. 7E). Although FB deficiency was associated with an increased intracellular bacterial burden (Fig. 7F), phosphorylated Akt levels were decreased (Fig. 7G), suggesting a putative mechanism for the increased cell

Downloaded from https://www.science.org at University of Massachusetts Worcester on February 08, 2023

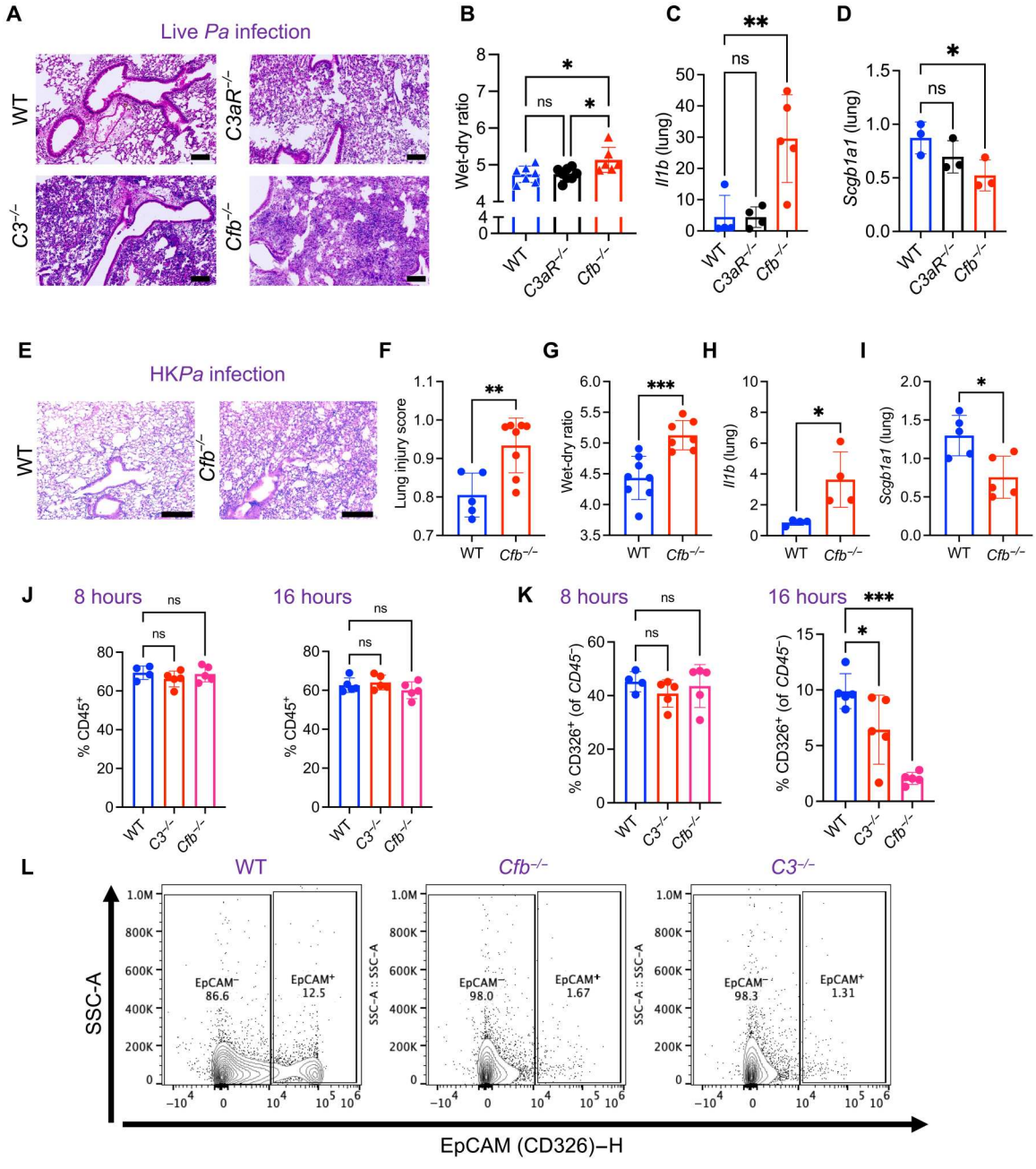

Fig. 5. Complement FB protects against stress-induced epithelial injury in vivo. (**A** to **D**) Global FB-deficient ($Cfb^{-/-}$) and C3aR-deficient ($C3aR^{-/-}$) B6 mice euthanized 24 hours after live *Pa* infection. (A) Representative images [$n = 5$ per group; scale bars (black), 100 μm]. These images are compared with WT and $C3^{-/-}$ mice from Fig. 1A because the lungs were obtained at the same time. (B) Wet-dry ratio. (C) *Il1b* expression normalized to *Hprt1*. (D) *Scgb1a1* expression normalized to *Gapdh*. (**E** to **I**) $Cfb^{-/-}$ and WT mice administered with HK*Pa* and euthanized 24 hours after infection. (E) Representative images [$n = 5$ per group; scale bars (black), 250 μm] with (F) differences in lung injury scores. These images should be compared with Fig. 1F because the lungs were obtained at the same time. Comparison of (G) lung wet-dry ratios and qRT-PCR for (H) *Il1b* and (I) *Scgb1a1*, both normalized to *Hprt1*. All qRT-PCR data were normalized to *Hprt1*. Flow cytometric analysis conducted on the lungs of WT, $C3^{-/-}$, and $Cfb^{-/-}$ mice euthanized 8 hours (**J**) and 16 hours (**K** and **L**) after *Pa* infection. Immune cell infiltration represented as percentage of $CD45^+$ cells and epithelial cell numbers represented by percentage of $CD45^-EpCAM(CD326)^+$ cells. Representative contour plots show $EpCAM^-$ and $EpCAM^+$ populations (gated on $CD45^-$ cells). Distribution of data is represented as scatterplots showing individual data points, and bars represent means ± SD. $^*P < 0.05$, $^{**}P < 0.01$, and $^{***}P < 0.001$ using unpaired two-tailed *t* test for two-group comparisons and ordinary one-way ANOVA with Dunnett's multiple comparisons testing for more than two groups [Šidák's for (B)].

Downloaded from https://www.science.org at University of Massachusetts Worcester on February 08, 2023

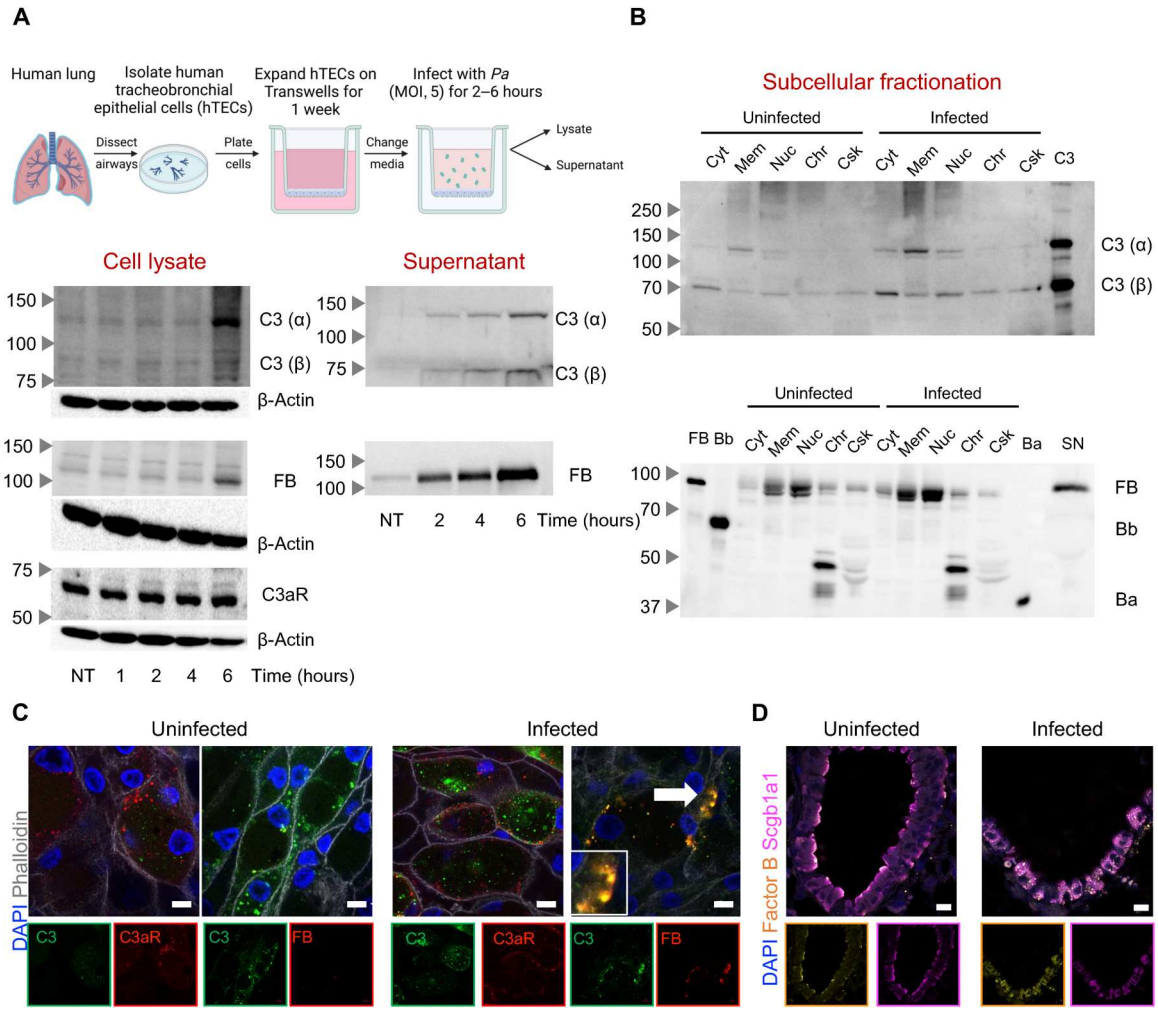

Fig. 6. Intracellular complement FB is up-regulated in primary human airway epithelial cells and in mouse lungs in vivo during *Pa* infection. (**A**) Immunoblots of C3, FB, and C3aR expression in primary hTECs infected with *Pa* (MOI, 5). Molecular weights in brackets. Protein shown from both cell lysate and apical supernatant from the Transwells. (**B**) Subcellular fractionation of uninfected primary hTECs and those at 4 hours after infection from the same donor, probed for C3 (top) and FB (bottom). Cyt, cytoplasmic extract; Mem, membrane extract; Nuc, soluble nuclear extract; Chr, chromatin extract; Csk, cytoskeletal extract. Same quantity of protein was loaded in each well. (**C**) Immunostaining for C3, C3aR, and FB in uninfected and infected hTECs using confocal microscopy at ×63 (oil) magnification [scale bars (white), 10 μm]. Phalloidin was used to visualize F-actin and identify individual cells. Images from individual channels under each main figure. All experiments are representative of $n = 3$ non-diseased donors. (**D**) Immunofluorescence using confocal microscopy for FB (yellow), Scgb1a1 (pink), and DAPI (blue) in club cell–deficient *C3*$^{f/f}$; *Scgb1a1*-CreERT2$^{+/-}$ mice euthanized 24 hours after administration of either PBS (uninfected) or HK*Pa*. Images are from individual channels under each main figure and representative of $n = 3$ mice in each group. Scale bars (white), 10 μm. Schematic created with biorender.com.

death seen in FB deficiency. These findings suggest that intracellular FB facilitates lung epithelial cell survival under stress by mitigating programmed cell death.

The cytoprotective effect of FB under stress parallels that of C3

To compare the protective effects of FB in the context of the protective effects of C3, we conducted live-cell cytotoxicity assays over time. Both C3- and FB-deficient cells demonstrated decreased viability over time compared with their common parent clones (termed WT, which are C3 and FB sufficient) in the settings of *Pa* infection (Fig. 8A) and oxidative stress (Fig. 8B). Similar to what was observed in FB deficiency, C3 deficiency resulted in lower phosphorylated Akt and increased programmed cell death over time, evident by increased cleaved caspase-3 and cleaved PARP levels after *Pa* infection (Fig. 8C). To address whether epithelial cell–derived C3 is acting extracellularly or intracellularly, we blocked C3 secretion in FB-sufficient and FB-deficient cells using increasing doses of a protein transport inhibitor (PTI; Fig. 8, D to F). C3 and its cleavage products decreased in the supernatant and correspondingly increased within the cell (Fig. 8D). Inhibition of C3 secretion decreased *Pa*-induced cell death in FB-sufficient cells, as evidenced by decreased cleaved PARP levels over time (Fig. 8E). This protection was abolished in FB-deficient cells (Fig. 8F), suggesting the necessity of FB for the cytoprotective effects of C3 in airway epithelium.

Downloaded from https://www.science.org at University of Massachusetts Worcester on February 08, 2023

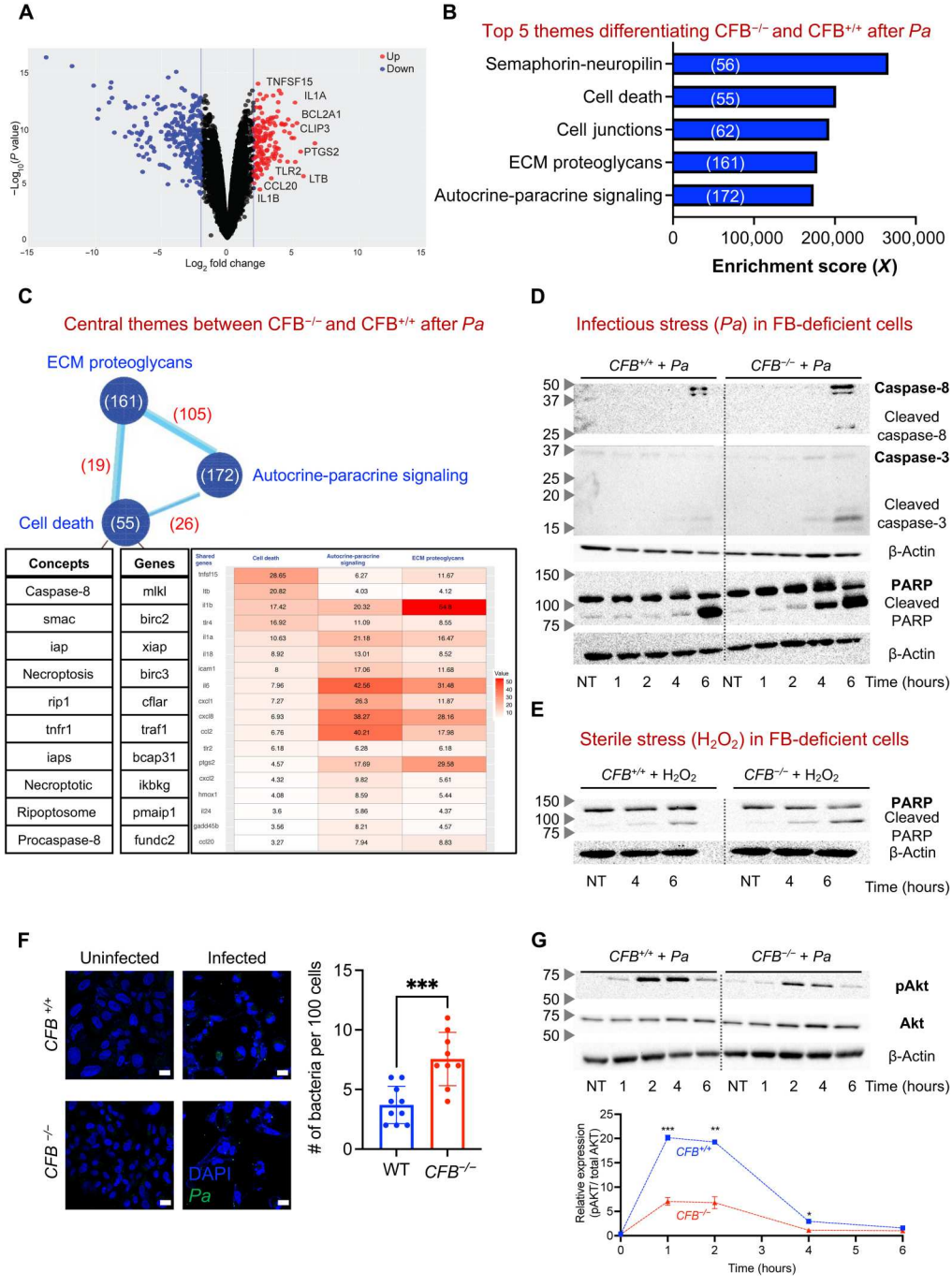

Fig. 7. Complement FB protects against stress-induced epithelial injury in vitro. (**A**) RNA-seq analysis conducted on infected human BEAS-2B cells (*Pa*; MOI, 5; harvested at 4 hours) rendered deficient in FB using CRISPR ($CFB^{-/-}$) versus their FB-sufficient parent clones ($CFB^{+/+}$). Volcano plot obtained from DESeq2 analysis showing fold change ($\log_2$) in gene expression, plotted against significance [$-\log_{10}$(*P* value)]. Red, significantly up-regulated gene; blue, significantly down-regulated genes (fold change > 2; $P < 0.05$). (**B**) A bar graph based on the analysis from (A) with the top five significant themes plotted by their enrichment scores (*x* axis) for the comparison using COMPBIO [the numbers of genes mapping to these themes are indicated in parentheses; all five have $P < 0.001$, which indicates the chance of seeing the theme (genes and concepts) in a random set of genes of the input size]. (**C**) Interrelationship between the three central themes from (B). Shared genes between themes are indicated in parentheses. The top 10 central concepts and genes for the cell death theme are shown in the accompanying table. The complete process map is shown in fig. S6. The pseudo heatmap shows the 18 shared genes common to all three themes and their contribution in each theme. The numeric values indicate the enrichment score of the genes. (**D**) Immunoblot analysis of caspase-8, caspase-3, PARP, and β-actin in $CFB^{-/-}$ and $CFB^{+/+}$ cells after *Pa* infection. Arrows denote cleaved fragments. (**E**) Similar immunoblot of cleaved PARP in $CFB^{-/-}$ and $CFB^{+/+}$ cells treated with H_2O_2 (250 μM). (**F**) Confocal microscopy images of $CFB^{-/-}$ and $CFB^{+/+}$ cells infected with FITC-tagged *Pa* (green) and fixed 4 hours after infection. Graph shows the number of bacteria per 100 cells counted. Scale bars (white), 20 μm. (**G**) Immunoblot analysis of pAkt, Akt, and β-actin in $CFB^{-/-}$ and $CFB^{+/+}$ cells after *Pa* infection, as well as densitometry analysis of $n = 3$ per group. Distribution of data is represented as scatterplots showing individual data points, and bars represent means ± SD.
$^{***}P < 0.001$, $^{**}P < 0.01$, and $^{*}P < 0.05$ using unpaired two-tailed *t* test.

DISCUSSION

The effects of the complement system have historically been attributed to its presence in the circulation. However, our understanding of individual complement components being synthesized by tissues and extrahepatic organs has evolved to recognize that cells at mucosal surfaces may have an intrinsic complement system for host defense (*40*–*44*). Leveraging advances in complement biology, model systems, and technologies, we demonstrate that (i) C3 protects against acute bacterial pneumonia–induced lung injury; (ii) C3 can be sourced locally, independent of that derived from the liver and present in the circulation; (iii) structural cells of the lung, such as epithelial cells, contribute to local C3 activity; (iv) epithelial cell–derived C3 protects against severe bacterial pneumonia; and (v) this protection is potentially occurring via intracellular complement FB, akin to canonical extracellular complement activation (*39*), but with important physiological functions necessary for cell survival. These observations put into perspective a long-standing premise that complement—an evolutionarily conserved defense system—may have originated intracellularly and evolved extracellularly with the complexity of the host (*45*).

Downloaded from https://www.science.org at University of Massachusetts Worcester on February 08, 2023

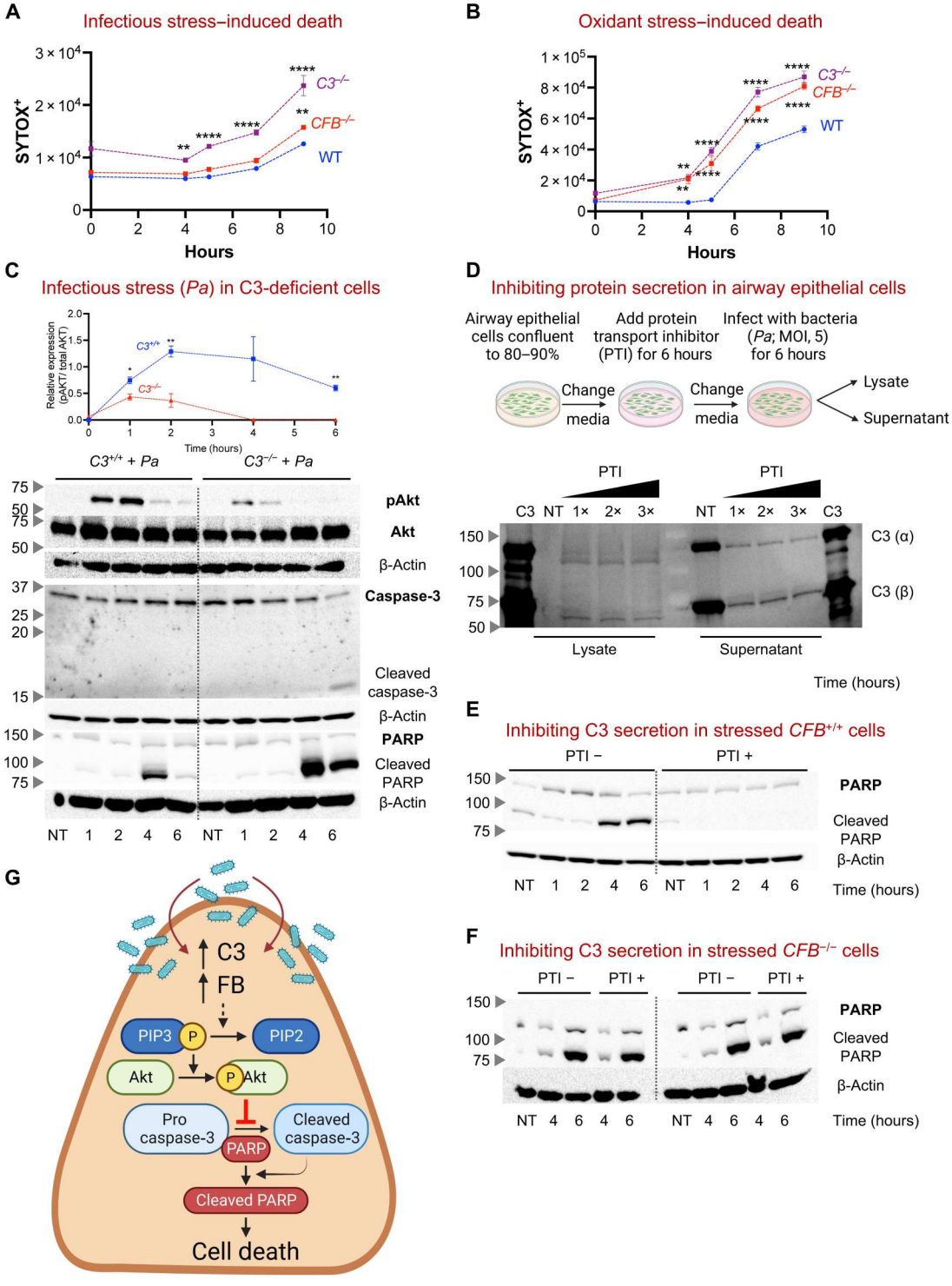

Fig. 8. The cytoprotective effect of FB under stress parallels that of C3. Cytotoxicity assays using high-content screening done using WT, *C3*-deficient (*C3*$^{-/-}$), and *CFB*-deficient (*CFB*$^{-/-}$) BEAS-2B cells in the setting of *Pa* infection (MOI, 2.5) (**A**) and oxidant stress [H_2O_2 (250 μM)] (**B**). *Y* axis represents the mean total intensity of SYTOX staining (n = 5 replicates in each group). The object identification (primary mask) is represented in blue, whereas SYTOX fluorescence is represented in red. (**C**) Immunoblot analysis of pAkt, Akt, caspase-3, PARP, and β-actin in *C3*$^{-/-}$ cells and their parent clones (*C3*$^{+/+}$) after *Pa* infection (MOI, 5). Arrows denote cleaved fragments. (**D**) *C3*$^{+/+}$ cells (nontreated, NT) treated with a protein transport inhibitor (PTI) cocktail at increasing concentrations, showing increased C3 accumulation intracellularly and decreased C3 secretion over 6 hours. Immunoblot analysis of (**E**) *CFB*$^{+/+}$ cells and (**F**) *CFB*$^{-/-}$ cells before and after *Pa* infection (MOI, 5) in the presence or absence of PTI. (**G**) Schematic diagram of how C3 and FB are up-regulated intracellularly during *Pa* infection, with a putative mechanism for reducing cell death. Distribution of data is represented as scatterplots showing individual data points, and bars represent means ± SD. *P < 0.05, **P < 0.01, and ****P < 0.0001 on ordinary one-way ANOVA test with multiple comparisons testing. Schematic figures were created with biorender.com.

Downloaded from https://www.science.org at University of Massachusetts Worcester on February 08, 2023

Liver-derived complement proteins form a necessary component of host defense, as evidenced by recurrent infections in patients with cirrhosis (*11*, *46*). To that effect, we found that splenic dissemination of bacteria was higher in the mice deficient in liver-derived C3 compared with controls, suggesting its role in enhancing immune resistance. However, there are two specific issues in this context that need consideration: first, that functional complement activity was observed in the BAL fluid of mice deficient in liver-derived C3 in the setting of infection despite no activity in the circulation and, second, that splenic bacterial burden in the mice deficient in liver-derived C3 was significantly lower than that observed in global C3-deficient mice. These observations would suggest that extrahepatic sources of C3 are induced and are important in controlling bacteremic pneumonia.

We and others have previously reported that lung epithelial cells produce and secrete C3, and this secretion is apically polarized, which may facilitate host defense at the air-liquid interface (*18*, *21*, *47*, *48*). Given our finding that C3 is up-regulated in lung epithelial cells under stress in vitro and in the infected airways of people with cystic fibrosis (*18*), we genetically depleted C3 specifically from lung epithelial cells that are known to be major sources of C3, Scgb1a1$^+$ club cells (*49*). The severity of bacterial pneumonia in these mice suggests that lung epithelial cell–derived C3 is necessary for protection against lung injury despite adequate circulating C3 levels. Cell-intrinsic C3 thus affects fundamental cellular processes such as survival, which until now had primarily been demonstrated in vitro (*18*, *19*).

Lung epithelial cells contain multiple intracellular complement components (*18*, *21*, *50*), yet which of these components offer cytoprotection in the *Pa* model along with cell-intrinsic C3 is unclear. Our findings indicate that intracellular FB is necessary for cellular survival. Our data also suggest that both C3 and FB promote Akt phosphorylation, which is known to inhibit lung epithelial cell death (*51*, *52*). However, we acknowledge that we have not yet identified the exact mechanism by which C3 connects to intracellular FB to promote cell survival. One possibility may be through the formation of an intracellular C3 convertase with C3b (C3bBb), as has been previously shown by other investigators (*21*, *53*). Whether this convertase facilitates clearance of intracellular pathogens or debris and how C3 and FB promote phospho-Akt (pAkt) signaling will be dissected in future work.

Given that C3a-C3aR interactions have been shown to facilitate the differentiation of naïve CD4$^+$ T cells toward a T helper cell 1 phenotype (*50*), alter mitochondrial calcium uptake and adenosine triphosphate production in stressed retinal pigment epithelial cells (*54*), and promote glucose-induced insulin secretion in human and mouse pancreatic islet cells (*19*, *55*), our findings on the cytoprotective role of FB suggest that intracellular C3 may have multiple targets and functions based on the stressor and the cell type. Moreover, although we have focused on FB in lung epithelial cells, other complement components have also been shown to modulate lung epithelial cell responses. For example, airway epithelial cells and alveolar (type 1 and type 2) epithelial cells also express C3aR, C5, C5aR1, and C5aR2, in addition to C3 and FB (*22*, *56*, *57*). C3aR activation on alveolar type 2 epithelial cells has recently been implicated in promoting endoplasmic reticulum stress and exacerbating bleomycin-induced lung injury, cellular apoptosis, and inflammation, which was suppressed by decay-accelerating factor (CD55) induction, a membrane-associated complement regulator (*58*). These observations create a precedent for complement modulating certain cellular processes in a stimuli-specific and cell-specific manner and accordingly targeting therapies on the basis of the desired effect.

There are certain limitations of our study. First, we deleted C3 from Scgb1a1$^+$ cells on the basis of our prior findings that (i) these cells are an abundant source of C3 (*18*), (ii) C3 protects both epithelial and alveolar cells from infection (*59*), and (iii) *Pa* infection induces bronchopneumonia (*60*). Future work will need to address whether the protective effects of lung epithelial cell–derived C3 in severe bacterial pneumonia are due to biosynthesized C3 that is stored in cells or is secreted by neighboring lung epithelial cells and is internalized (*18*, *24*). Second, there are sources of C3 in the lungs other than lung epithelial cells, such as monocyte/macrophages, fibroblasts, and mesenchymal stem cells (*17*, *61*–*63*). Future studies would determine whether delivering C3 to the lung via these other sources is sufficient for mitigating lung injury in a paracrine manner. Third, our findings are mainly from genetically altered murine models and primary hTEC cultures. We did not use recombinant complement proteins or pharmacologic inhibitors in vivo because we were focusing on biosynthesized intracellular stores; however, future work using cell-permeable inhibitors will help dissect the relative contributions of these stores to cellular function. Moreover, our current in vivo models lack the ability to detect the specific isoform of cytoprotective C3. There is increasing acknowledgement of a secreted form of C3 that has a signal peptide versus an intracellular cytosolic form with an alternate start site downstream of the signal peptide (*19*). Distinguishing these two forms of C3 may have therapeutic implications. In addition, although we have shown that C3 may be exerting its protective effect through FB, we do not exclude noncanonical intracellular interactions, such as how C3 interacts with ATG16L1 in pancreatic β cells (*19*) or in gut epithelial cells, thereby targeting the intracellular bacteria toward autophagolysosomes for degradation (*13*). Last, we focused on the role of C3 in acute injury due to bacterial pneumonia (i.e., within 24 hours). The effects of C3 may be different based on the stressor (*21*, *64*, *65*) and the temporal course of an infection (*66*).

In summary, we show that in addition to liver-derived C3, lung epithelial cell–derived C3 supports the host response to pneumonia by promoting both immune resistance and tissue resilience. This protection appears to occur via FB, which is an important component of the alternative pathway of the complement cascade (*67*). Our observation of an intracellular FB protein adds to the growing knowledge of how intracellular complement proteins modulate fundamental processes such as cell survival (*12*, *13*, *18*, *50*, *55*) and provides a putative mechanism by which lung epithelial cell–derived C3 offers protection. An understanding of tissue-derived and intracellular complement proteins is necessary to reconcile prior trial results of complement therapeutics, a majority of which have primarily targeted circulating complement proteins and do not necessarily penetrate inside the cell (*68*, *69*). We are optimistic that complement therapies targeting a specific organ can be reevaluated in terms of local protein activity and caution against the unintentional effects of cell-permeable complement inhibitors. In this manner, we will be able to harness endogenously produced immune mediators including the complement system to better combat diseases such as pneumonia-induced lung injury.

Downloaded from https://www.science.org at University of Massachusetts Worcester on February 08, 2023

MATERIALS AND METHODS

Study design

The primary objective of the research was to assess whether C3 deficiency increases the risk of severe pneumonia occurring in *Pa* infection. The secondary objectives included (i) assessing whether mice deficient in liver-derived C3 and mice deficient in lung epithelial cell–derived C3 were at increased risk of severe pneumonia compared with their littermate controls and (ii) whether the protective effects of C3 occurred via C3aR and/or FB. We used *Pa* as a model because it induces an acute bronchopneumonia (*9*). To eliminate the effects attributable to bacterial proliferation, we repeated in vivo experiments using HK*Pa*. For serum reconstitution experiments, NMS was administered intraperitoneally to C3-deficient mice. Mouse experiments included at least five mice in each group unless animal death occurred during the procedure. Each experiment was repeated at least twice, in most cases, by two independent authors. The effect was not attributed to differences between groups unless specified. Primary cell culture experiments included at least three different donors. RNA-seq experiments from BEAS-2B cells included three samples in each group. To evaluate whether the cytoprotective effects of C3 observed during an acute infection also occur in sterile injury, we used an in vitro model of oxidative stress (*18*).

Mice

All animal studies were conducted on protocols approved by the Institutional Animal Care and Use Committee at Washington University School of Medicine (WUSM). A table following the Animal Research: Reporting of In Vivo Experiments (ARRIVE) guidelines (*70*) for standard reporting of animal studies is included in the Supplementary Materials (table S1). All data are reported from controlled laboratory experiments. Mice (8 to 12 weeks of age) on a C57BL/6 background were used for all experiments. Commercially available mice (Jackson Laboratories, Bar Harbor, ME) purchased included WT C57BL/6J (WT, 000664) and B6.Cg-*Speer6-ps1*$^{Tg(Alb\text{-}cre)21Mgn}$/J (Alb-Cre, 003574) mice. *C3*-deficient, *C3aR*-deficient, and *Cfb*-deficient mice were maintained in colonies at WUSM (*67*, *71*–*74*). Scgb1a1-CreERT2$^{+/-}$ mice were generated by breeding an Scgb1a1-CreER^{TM} [B6N.129S6(Cg)-*Scgb1a1*$^{tm1(cre/ERT)Blh}$/J, strain no. 016225] to an Ai9 mouse [B6.Cg-*Gt(ROSA)26Sor*$^{tm9(CAG\text{-}tdTomato)Hze}$/J, strain no. 007909]. *C3*$^{f/f}$IRES-tdTomato mice were obtained from C. Kemper at the National Institutes of Health (*17*) and bred with Alb-Cre mice to create mice deficient in liver-derived C3 and with Scgb1a1-CreERT2$^{+/-}$ mice to generate mice deficient in lung epithelial cell–derived C3. Tail tips of mice were collected before weaning. Oligomers for polymerase chain reaction (PCR) amplification were designed to yield products of unique size to identify deleted sequences from *C3*, *C3aR*, and *Cfb* as previously published (*73*, *74*). PCR for digested tail samples was as follows: step 1 at 94°C for 4 min, step 2 at 94°C for 1 min, step 3 at 68°C for 1 min, step 4 at 72°C for 1 min, and steps 2 to 4 repeated for 30 cycles, followed by step 5 at 72°C for 5 min, and the reaction was concluded at 4°C until samples were retrieved. Primers used are listed in table S3. PCR products were visualized by electrophoresis using 2 to 3% agarose (#16500500, Thermo Fisher Scientific) gel with SYBR Safe dye (#S33102, Thermo Fisher Scientific).

Primary human epithelial cells, cell lines, and cell culture conditions

Human tissue use has been reviewed by the WUSM Institutional Review Board. Primary hTECs and BEAS-2B lung epithelial cells (CRL-9609, American Type Culture Collection, Manassas, VA) were used for in vitro experiments. The method for cell culture, including media composition, has been described (*18*). FB-deficient and C3aR-deficient BEAS-2B cells were generated by CRISPR nuclease-induced targeted double-strand break at the Genome Engineering Center at WUSM. *CFB* was disrupted by introducing out-of-frame indels in all alleles so that the mRNA would be degraded by nonsense-mediated decay (fig. S5A). *C3aR* only has one coding exon; hence, the gene was knocked out using two guide RNAs to delete the whole open reading frame (fig. S5B). These cells were confirmed to be *Mycoplasma* negative before experimentation and were compared with their parent clones in all experiments.

Preparation of bacteria for infection

Pa M57-15, a clinically relevant strain obtained from the sputum of a patient with cystic fibrosis (*75*), was cultured on LB agar plates (#L7025-500TAB, Sigma-Aldrich) overnight at 37°C from frozen stock. The next day, *Pa* was inoculated in LB broth (#L3522, Sigma-Aldrich) overnight at 37°C in a rotating shaker (220 rpm). The bacteria were recovered by centrifugation (3000*g*, 6 min, and 4°C) and resuspended in PBS. The absorbance at 380 nm (Epoch Microplate Spectrophotometer, BioTek) was used to quantify the required dose.

In vivo bacterial infection

Mice were infected with *Pa* for 8, 16, or 24 hours at a dose of 2×10^5 colony-forming units (CFU)/g of body weight, as stated in the figure legends, before euthanasia for blood and tissue harvest. To prepare HK*Pa*, stock solution was incubated at 100°C for 30 min and frozen at −80°C until use. Mice were anesthetized with a cocktail of ketamine (100 mg/kg) and xylazine (10 mg/kg) intraperitoneally and then orotracheally intubated using a fiber-optic cable connected to a light source (BioLITE Intubation System, BIO-MI-KIT, Braintree Scientific, Braintree, MA) to facilitate the insertion of a Surflo 20-gauge catheter (#SR-OX2025CA, Terumo Medical Products, Somerset, NJ) within the trachea. The suspension of bacteria in sterile PBS was introduced into the catheter at a volume of 1 μl/g of body weight. Euthanasia was carried out using Avertin [2% working solution of Avertin is prepared from 100% Avertin, which is made by mixing 1 g of 2,2,2-tribromoethyl alcohol (#T48402, Sigma-Aldrich) with 1 ml of *tert*-amyl alcohol (#240486, Sigma-Aldrich)]. Lungs were harvested either for the wet-dry ratio, BAL collection, flow cytometry, or bacterial colony counts or as a whole organ for fixation in 10% formalin before submission for histology. Spleens were harvested for colony counts. BAL was collected from mouse lungs using 0.5 to 1 ml of PBS with 1× Halt Protease Inhibitor Cocktail (diluted from 100×; #78429, Thermo Fisher Scientific). After collection, BAL was spun down at 500*g* for 5 min before supernatant was collected and stored at −80°C for further experiments.

In vitro stress-induced epithelial injury

For in vitro infection, *Pa* M57-15 was used at different multiplicities of infection (MOIs) and for different periods of time, as indicated in the figure legends. Bacterial cultures were suspended in DMEM (Dulbecco's modified Eagle's medium; #10-017-CV, Corning, NY)

Downloaded from https://www.science.org at University of Massachusetts Worcester on February 08, 2023

supplemented with 10% heat-inactivated antibiotic-free fetal bovine serum (#26140079, Thermo Fisher Scientific). For in vitro oxidative stress experiments, hydrogen peroxide (H_2O_2; H1009, Sigma-Aldrich, St. Louis, MO) was freshly prepared to a concentration of 250 to 1000 μM before use. To separate the effects of proteins acting extracellularly versus their intracellular roles, we inhibited protein secretion by treating epithelial cells using a PTI cocktail [#00-4980, eBioscience Protein Transport Inhibitor Cocktail (500×)] containing brefeldin A and monensin. Cells were plated in a 35-mm plate at a density of 5×10^5 cells/ml per plate 24 hours before treatment. At 80 to 90% confluence, cells were washed with PBS and then treated with 1× PTI (directly added to culture medium) for 6 hours. This was followed by *Pa* infection (MOI, 5). The supernatant and lysate were collected from these cells, and inhibition of protein secretion was confirmed through immunoblotting. Details regarding RNA extraction and sequencing and analysis of RNA-seq data from BEAS-2B cells have also been provided in Supplementary Methods. Differentially expressed genes (1.6-fold, adjusted *P* value of <0.05) were further analyzed by a knowledge engine called COMPBIO (V2.0) (*76*).

Intracellular bacterial burden

BEAS-2B cells were plated 1 day before infection on a glass coverslip in a 12-well plate at a density of 1.5×10^5/ml per well. For preparing fluorescein isothiocyanate (FITC)–labeled *Pa*, FITC (#46950, Sigma-Aldrich) was dissolved in anhydrous dimethyl sulfoxide to a working concentration of 500 μg/ml. *Pa* was prepared as described above and suspended in 1 ml of sterile PBS. From a working concentration (500 μg/ml), 5 μl of FITC were added to 1 ml of bacterial culture, followed by gentle rotation at room temperature for 60 min protected from light to label the bacteria. The bacterial pellet was subsequently harvested by centrifugation at 3000*g* for 5 min at room temperature, followed by washing twice in sterile PBS. The pellet was suspended in antibiotic-free DMEM for infection. After 4 hours of infection, cells were incubated for 60 min in DMEM containing gentamicin (10 μg/ml; #15750-060, Gibco) to remove extracellular bacteria. Cells were then washed twice with PBS, fixed, and stained with DAPI (4′,6-diamidino-2-phenylindole) before confocal microscopy on a Zeiss LSM 880 laser scanning confocal microscope (Carl Zeiss Inc., Thornwood, NY) at ×63 oil magnification.

Assessment of functional fluid-phase complement activity

We adapted a previously published assay for serum (*27*). For its use with BAL, enzyme-linked immunosorbent assay (ELISA) plates (96-well flat-bottom; #3855, Thermo Fisher Scientific) were coated with LPS (2 μg per well in 100 μl; #L2762, Sigma-Aldrich) overnight at 4°C. After washing three times with a solution of 0.05% Tween 20 in PBS, samples (serum, 1:10 and BAL, 1:5) in Mg^{2+}-EGTA buffer were added (50 μl per well) and incubated at 37°C for 1 hour. The plates were washed again three times, and goat anti-mouse C3 (100 μl per well; #55463, MP Biomedicals) diluted in 1% bovine serum albumin (BSA; #A7906, Sigma-Aldrich) in PBS (1:4000 in 1% BSA/PBS) was added for 1 hour. After another three washes, samples were incubated with horseradish peroxidase–conjugated donkey anti-goat immunoglobulin G antibody (100 μl per well; 1:2000 in 1% BSA/PBS; #705-035-147, Jackson ImmunoResearch Laboratories) for 1 hour. After three washes, TMB Color Substrate (#DY999, R&D Systems) was added at 100 μl per well and incubated at room temperature for 10 min. The reaction was stopped by addition of 1 M sulfuric acid (50 μl per well; #DY994, R&D Systems), and optical density was measured at 450 nm (Epoch Microplate Spectrophotometer, BioTek).

Assessment of ALI and infection severity

ALI was assessed using multiple domains (*77*). To assess club cell death in vivo, we quantified Scgb1a1$^+$ cells in the terminal bronchioles in a fixed 150-μm length of the airway in multiple, independent areas of the lung. Acetylated α-tubulin was used to identify ciliated cells. A "club cell ratio" was obtained by dividing the club cell numbers (Scgb1a1$^+$) by the sum of the club cells (Scgb1a1$^+$) + ciliated cells (acetylated α-tubulin$^+$) in the same fixed length of airway (*36*–*38*). To obtain a wet-dry ratio, we immediately measured the weight of "wet" lungs after euthanasia (#AB54-S, Mettler Toledo, Columbus, OH), and the value obtained was divided by their "dry" weight that was measured after 24 hours in a 65°C oven. To assess physiological dysfunction, we performed whole-body plethysmography as previously described (*78*). Changes in airway resistance (RI) and dynamic compliance (C_{dyn}) were recorded in response to increasing doses of inhaled methacholine (#A2251, Sigma-Aldrich). To assess systemic bacterial burden, spleens were harvested into 0.9 ml of sterile PBS and homogenized in microtubes (#72.694.006, Sarstedt AG & Co, Nümbrecht, Germany) using stainless steel beads (11079132ss, BioSpec, Bartlesville, OK) on a bead beater. The homogenate was serially diluted, plated on LB agar, and incubated at 37°C overnight before colony counting. To assess local bacterial burden, lungs were harvested into 0.8 ml of sterile PBS and processed similarly. The total volume of both spleen and lung homogenate was 1 ml.

Flow cytometry

To obtain a single-cell suspension, mouse lungs were digested using collagenase A (1.5 mg/ml; 10103586001, Roche), deoxyribonuclease I (0.1 mg/ml; D4527, Sigma-Aldrich), 5% fetal bovine serum, 10 mM Hepes buffer (25-060-CI, Corning, Durham, NC), and PBS. Specifically, after perfusing the right atrium with 10 ml of 1× PBS, the lungs were inflated with 1 ml of the abovementioned digest solution, cut into 3- to 4-mm pieces using scissors, and gently vortexed in 2 ml of digest solution. The digest was incubated at 37°C for 40 min in a shaker incubator at 190 rpm while gently vortexing the samples every 5 to 7 min. After adding 10 ml of ice-cold PBS, the digest was vortexed for 30 s, filtered through a 70-μm strainer (431751, Corning), and spun at 500*g* for 10 min at 4°C. After discarding the supernatant, the cells were resuspended in 2 ml of ACK Lysing Buffer (A10492-01, Gibco) and incubated at room temperature for 4 to 7 min, after which they were resuspended in 10 ml of ice-cold 1% BSA in PBS and centrifuged again at 500*g* for 10 min at 4°C. A total of 1×10^6 to 2×10^6 cells were added to a 96-well plate for staining using antibodies listed in table S2. Data were acquired on an Attune NxT flow cytometer (Thermo Fisher Scientific) and analyzed using FlowJo v10.8.0 (Becton, Dickinson and Company, Ashland, OR).

Cytokine and chemokine measurements

Serum was obtained before and after infection from the same mice; however, BAL was obtained from different mice in the uninfected and infected groups because the BAL procedure is terminal. For BAL protein levels [i.e., bicinchoninic acid (BCA) assay], fresh or thawed BAL samples were diluted (1:10 to 1:50 in PBS) to fall within the range of the recommended standard curve of the assay

Downloaded from https://www.science.org at University of Massachusetts Worcester on February 08, 2023

before total protein level was quantified using the Pierce BCA Protein Assay Kit (#23227, Thermo Fisher Scientific) according to the provided protocol. To assess cytokine levels in mouse serum and BAL, we used a multianalyte assay (LEGENDplex Mouse Inflammation Panel; #740446, BioLegend, San Diego, CA) according to the provided protocol. To assess epithelial cell injury in the mouse BAL, we used Mouse RAGE DuoSet ELISA (#DY1179, R&D Systems, Minneapolis, MN) according to the provided protocol. The BAL samples were either diluted 1:2 or 1:4 on the basis of known protein levels, but in a single run, the dilutions were the same. To assess epithelial cell death in mouse BAL, we used Mouse Cytokeratin 18 ELISA (#ab243678, Abcam, Cambridge, UK) according to the provided protocol. BAL samples were diluted 1:2 for this assay.

Immunoblotting

Samples obtained from mice were diluted in PBS at a ratio of 1:10 for plasma and 1:5 for BAL. Laemmli sample buffer (1610747, Bio-Rad, Hercules, CA) was added to each sample and boiled for 5 min at 100°C in a heat block for complete denaturation of protein. To prepare cell lysates for immunoblotting, cells were washed in ice-cold PBS and lysed using lysis buffer (9803, Cell Signaling Technology, Danvers, MA) supplemented with Halt Protease Inhibitor Cocktail (78429, Thermo Fisher Scientific, Waltham, MA) for 20 min on ice. Lysates were cleared by centrifugation (14,000*g*) for 10 min and cooked in SDS-denaturing Laemmli sample buffer for 5 min. Immunoblotting was done as previously described (*18*) using antibodies listed in table S2.

Immunostaining

Cells were plated on coverslips in 24-well plates at a seeding density of 10^5 cells per well overnight before the experiment. For evaluating the cellular response to *Pa* using immunostaining, cells were fixed by directly adding fixative solution [10% neutral-buffered formalin, prepared by mixing 100 ml of formaldehyde (37 to 40%), 900 ml of distilled water, sodium phosphate (monobasic; 4 g/liter), and sodium phosphate (dibasic, anhydrous; 6.5 g/liter)] equal in amount to the medium present in the well. After removing media and fixative solution after 2 min, 500 μl of fixative solution were again added to cells and incubated for 20 min at room temperature. The solution was aspirated, and cells were then washed twice with PBS. Cells were permeabilized by adding 0.05% Triton X-100 (T8787, Sigma-Aldrich, St. Louis, MO) in PBS for 5 min at room temperature, followed by washing twice with PBS. Cells were blocked by adding 2% BSA (9048-46-8, Santa Cruz Biotechnology) in PBS for 30 min at room temperature, followed by washing twice with PBS, and immunostaining was performed as previously described (*18*) using antibodies listed in table S2. Cells were imaged using a Zeiss LSM 880 laser scanning confocal microscope (Carl Zeiss Inc., Thornwood, NY) at ×63 oil magnification. Immunofluorescence staining of lungs was also performed as previously described (*18*) on tissue sections deparaffinized with xylene and ethanol using antibodies listed in table S2.

RNAScope in situ hybridization

RNAScope in situ hybridization was carried out using the ACD HybEZ II Hybridization System With ACD EZ-Batch Slide System (Advanced Cell Diagnostics, Newark, CA), following the protocol for Multiplex Fluorescent Reagent Kit v2 Assay (Advanced Cell Diagnostics) using probes for *Scgb1a1* (420351-C3) and *C3* (417841). Opal 520 (FP1487001KT, Akoya Biosciences, Marlborough, MA) was used for *Scgb1a1*, and Opal 650 (FP1496001KT) was used for *C3* (both 1:750); slides were imaged using a Zeiss LSM 880 laser scanning confocal microscope (Carl Zeiss Inc., Thornwood, NY) at ×63 oil magnification.

Live-cell imaging for cytotoxicity

H_2O_2-induced cytotoxicity was analyzed using an IncuCyte Live Cell Imager (Sartorius, Göttingen, Germany) at the Genome Engineering and iPSC Center at WUSM. The ratio of SYTOX Green Nucleic Acid Stain (1:10,000; S7020, Invitrogen) and SYTO 24 Green Fluorescent Nucleic Acid Stain (1:1000; S7559, Invitrogen) was reported over time and averaged over four independent fields in each well of a 96-well plate, with four technical replicates per time point. Infection-induced cytotoxicity was assessed using CellInsight CX5 High Content Screening (HCS) Platform with an on-stage incubator (maintained at 37°C and 5% CO_2). Cells were stained with 1× HCS NuclearMask Staining (#H10325, Thermo Fisher Scientific) and 1 μM SYTOX AADvanced Dead Cell Stain Kit (#S10274, Thermo Fisher Scientific) in DMEM supplemented with 1% penicillin/streptomycin, 1% glutamine, and 10% fetal bovine serum [CellInsight CX5 configuration: Assay Algorithm TargetActivation.V4; HCS NuclearMask (channel 1) was detected by filter 386-23, and the SYTOX AADvanced stain (channel 2) was detected by filter 560-25]. Cell viability was assessed by measuring the total intensity of SYTOX staining. Values shown are means ± SD of five replicate wells, which represent SYTOX total intensity of all pixels within an object [$^{***}P < 0.001$ and ns (not significant].

Quantitative reverse transcription PCR for inflammatory and epithelial cell genes

mRNA extraction was performed using an RNeasy Plus Mini kit (#74134, QIAGEN, Germantown, MD) as per the manufacturer's protocol, and complementary DNA (cDNA) synthesis was performed using the High-Capacity cDNA Reverse Transcription Kit (#4368814, Thermo Fisher Scientific) according to the manufacturer's recommendations. Each cDNA sample was diluted by fivefold after cDNA synthesis, and real-time PCR of each gene was carried out in duplicate on a Roche LightCycler 480 real-time PCR instrument. Each PCR contained 2 μl of cDNA template, 0.6 μl of forward and reverse primers (with a final concentration of 0.5 μM per well), 4 μl of SYBR Green master mix (A46109, Applied Biosystems), and 5.4 μl of reverse transcription PCR (RT-PCR)–grade H_2O. All primers were ordered from Integrated DNA Technologies (table S4). The PCR program was run as follows: an initial preincubation step at 95°C for 3 min followed by 45 cycles of denaturation at 95°C for 10 s, annealing and elongation at 60°C for 20 s, and fluorescence reading at 72°C for 1 s. C_t values were read and exported from LightCycler 480 software, and the commonly used $2(-\Delta\Delta C_t)$ method was used to calculate relative gene expression using *Gapdh* or *Hprt1* as the housekeeping gene. Data shown are adjusted to the housekeeping gene.

Single-cell RNA-seq analysis from LungMAP

The single-cell reference program for human lungs was used on the LGEA (LungMAP Phase 2) web portal (*29*–*32*) (available at https://research.cchmc.org/pbge/lunggens/tools/lung_at_glance.html?tab=reference). LungMAP was used to compare the relative

Downloaded from https://www.science.org at University of Massachusetts Worcester on February 08, 2023

expression of *C3* across different cell types (*x* axis) in nondiseased human lungs. Cell ontologies were obtained from the NHLBI Molecular Atlas of Lung Development Program Consortium (*79*). The expression of a gene in each cell type was measured using the total unique molecular identifier (UMI) counts for each cell divided by the median UMI counts per cell and normalized using "LogNormalize" in Seurat ("normalized expression," *y* axis). The LungMAP single-cell RNA-seq reference is associated with the Lung CellCards resource (*32*). This initial reference integrated 259,000 cells from 72 donors from five published (*80*–*84*) and one unpublished single-cell RNA-seq cohort. It consists of nondiseased adult and pediatric healthy lung single-cell 10x Genomics captures (v2 and v3).

Statistical analysis

Data are presented as scatterplots showing individual data points, and dispersion is shown by means ± SD. Unpaired *t* test was used for comparing two groups, assuming equal variance, and ordinary one-way analysis of variance (ANOVA) test with multiple comparisons testing was used for more than two groups. A P value of <0.05 was considered significant, although values of >0.05 have been reported when there was evidence of a trend. Prism v9.3.0 (GraphPad, San Diego, CA) was used for statistical analysis.

Supplementary Materials

This PDF file includes:
Methods
Figs. S1 to S6
Tables S1 to S4
References (*85*–*90*)

Other Supplementary Material for this manuscript includes the following:
Data file S1
MDAR Reproducibility Checklist

View/request a protocol for this paper from *Bio-protocol*.

REFERENCES AND NOTES

1. L. J. Quinton, A. J. Walkey, J. P. Mizgerd, Integrative physiology of pneumonia. *Physiol. Rev.* **98**, 1417–1464 (2018).
2. A. Torres, C. Cilloniz, M. S. Niederman, R. Menéndez, J. D. Chalmers, R. G. Wunderink, T. van der Poll, Pneumonia. *Nat. Rev. Dis. Primers* **7**, 25 (2021).
3. B. T. Thompson, R. C. Chambers, K. D. Liu, Acute respiratory distress syndrome. *N. Engl. J. Med.* **377**, 1904–1905 (2017).
4. M. A. Matthay, R. L. Zemans, G. A. Zimmerman, Y. M. Arabi, J. R. Beitler, A. Mercat, M. Herridge, A. G. Randolph, C. S. Calfee, Acute respiratory distress syndrome. *Nat. Rev. Dis. Primers.* **5**, 18 (2019).
5. C. S. Dela Cruz, S. E. Evans, M. I. Restrepo, N. Dean, A. Torres, I. Amara-Elori, S. Awasthi, E. Caler, B. Cao, J. D. Chalmers, J. Chastre, T. S. Cohen, A. H. Cohen, K. Crothers, Y. P. Di, M. E. Egan, C. Feldman, S. Gautam, E. S. Halstead, S. Herold, B. E. Jones, C. Luna, M. S. Niederman, R. Mendez, R. Menendez, J. P. Mizgerd, R. Nusrat, J. Ramirez, Y. Shindo, G. Waterer, S. M. Yeligar, R. G. Wunderink, Understanding the host in the management of pneumonia. An official American Thoracic Society workshop report. *Ann. Am. Thorac. Soc.* **18**, 1087–1097 (2021).
6. S. K. Sahu, D. H. Kulkarni, A. N. Ozanturk, L. Ma, H. S. Kulkarni, Emerging roles of the complement system in host-pathogen interactions. *Trends Microbiol.* **30**, 390–402 (2021).
7. W. Bain, H. Li, R. van der Geest, S. R. Moore, T. F. Olonisakin, B. Ahn, E. Papke, K. Moghbeli, R. DeSensi, S. Rapport, M. Saul, M. Hulver, Z. Xiong, R. K. Mallampalli, P. Ray, A. Morris, L. Ma, Y. Doi, Y. Zhang, G. D. Kitsios, H. S. Kulkarni, B. J. McVerry, V. P. Ferreira, M. Nouraie, J. S. Lee, Increased alternative complement pathway function and improved survival during critical illness. *Am. J. Respir. Crit. Care Med.* **202**, 230–240 (2020).
8. J. S. Brown, T. Hussell, S. M. Gilliland, D. W. Holden, J. C. Paton, M. R. Ehrenstein, M. J. Walport, M. Botto, The classical pathway is the dominant complement pathway required for innate immunity to Streptococcus pneumoniae infection in mice. *Proc. Natl. Acad. Sci. U.S.A.* **99**, 16969–16974 (2002).
9. S. L. Mueller-Ortiz, S. M. Drouin, R. A. Wetsel, The alternative activation pathway and complement component C3 are critical for a protective immune response against Pseudomonas aeruginosa in a murine model of pneumonia. *Infect. Immun.* **72**, 2899–2906 (2004).
10. Y. Okura, I. Kobayashi, M. Yamada, S. Sasaki, Y. Yamada, I. Kamioka, R. Kanai, Y. Takahashi, T. Ariga, Clinical characteristics and genotype-phenotype correlations in C3 deficiency. *J. Allergy Clin. Immunol.* **137**, 640–644.e1 (2016).
11. A. Albillos, R. Martin-Mateos, S. Van der Merwe, R. Wiest, R. Jalan, M. Álvarez-Mon, Cirrhosis-associated immune dysfunction. *Nat. Rev. Gastroenterol. Hepatol.* **19**, 112–134 (2022).
12. J. C. H. Tam, S. R. Bidgood, W. A. McEwan, L. C. James, Intracellular sensing of complement C3 activates cell autonomous immunity. *Science* **345**, 1256070 (2014).
13. M. T. Sorbara, E. G. Foerster, J. Tsalikis, M. Abdel-Nour, J. Mangiapane, I. Sirluck-Schroeder, I. Tattoli, R. van Dalen, D. E. Isenman, J. R. Rohde, S. E. Girardin, D. J. Philpott, Complement C3 drives autophagy-dependent restriction of cyto-invasive bacteria. *Cell Host Microbe* **23**, 644–652.e5 (2018).
14. M. Torisu, T. Yokoyama, P. F. Kohler, A. L. Durst, G. Martineau, G. Schroter, H. Amemiya, C. G. Groth, T. E. Starzl, Serum complement after orthotopic transplantation of the human liver. *Clin. Exp. Immunol.* **12**, 21–30 (1972).
15. B. J. C. Janssen, A. Christodoulidou, A. McCarthy, J. D. Lambris, P. Gros, Structure of C3b reveals conformational changes that underlie complement activity. *Nature* **444**, 213–216 (2006).
16. I. Charlie-Silva, A. Klein, J. M. M. Gomes, E. J. R. Prado, A. C. Moraes, S. F. Eto, D. C. Fernandes, J. J. Fagliari, J. D. C. Junior, C. Lima, M. Lopes-Ferreira, K. Conceição, W. G. Manrique, M. A. A. Belo, Acute-phase proteins during inflammatory reaction by bacterial infection: Fish-model. *Sci. Rep.* **9**, 4776 (2019).
17. M. Kolev, E. E. West, N. Kunz, D. Chauss, E. A. Moseman, J. Rahman, T. Freiwald, M. L. Balmer, J. Lötscher, S. Dimeloe, E. C. Rosser, L. R. Wedderburn, K. D. Mayer-Barber, A. Bohrer, P. Lavender, A. Cope, L. Wang, M. J. Kaplan, N. M. Moutsopoulos, D. McGavern, S. M. Holland, C. Hess, M. Kazemian, B. Afzali, C. Kemper, Diapedesis-induced integrin signaling via LFA-1 facilitates tissue immunity by inducing intrinsic complement C3 expression in immune cells. *Immunity* **52**, 513–527.e8 (2020).
18. H. S. Kulkarni, M. L. Elvington, Y.-C. Perng, M. K. Liszewski, D. E. Byers, C. Farkouh, R. D. Yusen, D. J. Lenschow, S. L. Brody, J. P. Atkinson, Intracellular C3 protects human airway epithelial cells from stress-associated cell death. *Am. J. Respir. Cell Mol. Biol.* **60**, 144–157 (2019).
19. B. C. King, K. Kulak, U. Krus, R. Rosberg, E. Golec, K. Wozniak, M. F. Gomez, E. Zhang, D. J. O'Connell, E. Renström, A. M. Blom, Complement component C3 is highly expressed in human pancreatic islets and prevents β cell death via ATG16L1 interaction and autophagy regulation. *Cell Metab.* **29**, 202–210.e6 (2019).
20. J. Friščić, M. Böttcher, C. Reinwald, H. Bruns, B. Wirth, S.-J. Popp, K. I. Walker, J. A. Ackermann, X. Chen, J. Turner, H. Zhu, L. Seyler, M. Euler, P. Kirchner, R. Krüger, A. B. Ekici, T. Major, O. Aust, D. Weidner, A. Fischer, F. T. Andes, Z. Stanojevic, V. Trajkovic, M. Herrmann, A. Korb-Pap, I. Wank, A. Hess, J. Winter, V. Wixler, J. Distler, G. Steiner, H. P. Kiener, B. Frey, L. Kling, K. Raza, S. Frey, A. Kleyer, T. Bäuerle, T. R. Hughes, A. Grüneboom, U. Steffen, G. Krönke, A. P. Croft, A. Filer, J. Köhl, K. Klein, C. D. Buckley, G. Schett, D. Mougiakakos, M. H. Hoffmann, The complement system drives local inflammatory tissue priming by metabolic reprogramming of synovial fibroblasts. *Immunity* **54**, 1002–1021.e10 (2021).
21. B. Yan, T. Freiwald, D. Chauss, L. Wang, E. West, C. Mirabelli, C. J. Zhang, E.-M. Nichols, N. Malik, R. Gregory, M. Bantscheff, S. Ghidelli-Disse, M. Kolev, T. Frum, J. R. Spence, J. Z. Sexton, K. D. Alysandratos, D. N. Kotton, S. Pittaluga, J. Bibby, N. Niyonzima, M. R. Olson, S. Kordasti, D. Portilla, C. E. Wobus, A. Laurence, M. S. Lionakis, C. Kemper, B. Afzali, M. Kazemian, SARS-CoV-2 drives JAK1/2-dependent local complement hyperactivation. *Sci. Immunol.* **6**, eabg0833 (2021).
22. N. Chaudhary, A. Jayaraman, C. Reinhardt, J. D. Campbell, M. Bosmann, A single-cell lung atlas of complement genes identifies the mesothelium and epithelium as prominent sources of extrahepatic complement proteins. *Mucosal Immunol.* **15**, 927–939 (2022).
23. H. S. Kulkarni, M. K. Liszewski, S. L. Brody, J. P. Atkinson, The complement system in the airway epithelium: An overlooked host defense mechanism and therapeutic target? *J. Allergy Clin. Immunol.* **141**, 1582–1586.e1 (2018).
24. M. Elvington, M. K. Liszewski, P. Bertram, H. S. Kulkarni, J. P. Atkinson, A C3(H20) recycling pathway is a component of the intracellular complement system. *J. Clin. Invest.* **127**, 970–981 (2017).
25. M. S. Bolger, D. S. Ross, H. Jiang, M. M. Frank, A. J. Ghio, D. A. Schwartz, J. R. Wright, Complement levels and activity in the normal and LPS-injured lung. *Am. J. Physiol. Lung Cell. Mol. Physiol.* **292**, L748–L759 (2007).
26. Y. Kimura, T. Miwa, L. Zhou, W.-C. Song, Activator-specific requirement of properdin in the initiation and amplification of the alternative pathway complement. *Blood* **111**, 732–740 (2008).
27. P. Bertram, A. M. Akk, H. Zhou, L. M. Mitchell, C. T. N. Pham, D. E. Hourcade, Anti-mouse properdin TSR 5/6 monoclonal antibodies block complement alternative pathway-dependent pathogenesis. *Monoclon. Antib. Immunodiagn. Immunother.* **34**, 1–6 (2015).

Downloaded from https://www.science.org at University of Massachusetts Worcester on February 08, 2023

28. X. Wu, I. Hutson, A. M. Akk, S. Mascharak, C. T. N. Pham, D. E. Hourcade, R. Brown, J. P. Atkinson, C. A. Harris, Contribution of adipose-derived factor D/adipsin to complement alternative pathway activation: Lessons from lipodystrophy. *J. Immunol.* **200**, 2786–2797 (2018).
29. Y. Du, M. Guo, J. A. Whitsett, Y. Xu, "LungGENS": A web-based tool for mapping single-cell gene expression in the developing lung. *Thorax* **70**, 1092–1094 (2015).
30. Y. Du, J. A. Kitzmiller, A. Sridharan, A. K. Perl, J. P. Bridges, R. S. Misra, G. S. Pryhuber, T. J. Mariani, S. Bhattacharya, M. Guo, S. S. Potter, P. Dexheimer, B. Aronow, A. H. Jobe, J. A. Whitsett, Y. Xu, Lung gene expression analysis (LGEA): An integrative web portal for comprehensive gene expression data analysis in lung development. *Thorax* **72**, 481–484 (2017).
31. Y. Du, W. Ouyang, J. A. Kitzmiller, M. Guo, S. Zhao, J. A. Whitsett, Y. Xu, Lung gene expression analysis web portal version 3: Lung-at-a-glance. *Am. J. Respir. Cell Mol. Biol.* **64**, 146–149 (2021).
32. X. Sun, A.-K. Perl, R. Li, S. M. Bell, E. Sajti, V. V. Kalinichenko, T. V. Kalin, R. S. Misra, H. Deshmukh, G. Clair, J. Kyle, L. E. Crotty Alexander, J. M. Silva, J. A. Kitzmiller, K. A. Wikenheiser-Brokamp, G. Deutsch, M. Guo, Y. Du, M. P. Morley, M. J. Valdez, H. V. Yu, K. Jin, E. E. Bardes, J. A. Zepp, T. Neithamer, M. C. Basil, W. J. Zacharias, J. Verheyden, R. Young, G. Bandyopadhyay, S. Lin, C. Ansong, J. Adkins, N. Salomonis, B. J. Aronow, Y. Xu, G. Pryhuber, J. Whitsett, E. E. Morrisey; NHLBI LungMAP consortium, A census of the lung: CellCards from LungMAP. *Dev. Cell* , 112–145.e2 (2021).
33. L. S. Van Winkle, A. R. Buckpitt, C. G. Plopper, Maintenance of differentiated murine Clara cells in microdissected airway cultures. *Am. J. Respir. Cell Mol. Biol.* **14**, 586–598 (1996).
34. M. V. Fanucchi, M. E. Murphy, A. R. Buckpitt, R. M. Philpot, C. G. Plopper, Pulmonary cytochrome P450 monooxygenase and Clara cell differentiation in mice. *Am. J. Respir. Cell Mol. Biol.* **17**, 302–314 (1997).
35. A. Guha, M. Vasconcelos, Y. Cai, M. Yoneda, A. Hinds, J. Qian, G. Li, L. Dickel, J. E. Johnson, S. Kimura, J. Guo, J. McMahon, A. P. McMahon, W. V. Cardoso, Neuroepithelial body microenvironment is a niche for a distinct subset of Clara-like precursors in the developing airways. *Proc. Natl. Acad. Sci. U.S.A.* **109**, 12592–12597 (2012).
36. B. M. Henry, I. Cheruiyot, S. W. Benoit, F. Sanchis-Gomar, G. Lippi, J. Benoit, Cytokeratin 18 cell death assays as biomarkers for quantification of apoptosis and necrosis in COVID-19: A prospective, observational study. *J. Clin. Pathol.* **75**, 410–415 (2021).
37. J.-H. Pan, T. L. Adair-Kirk, A. C. Patel, T. Huang, N. S. Yozamp, J. Xu, E. P. Reddy, D. E. Byers, R. A. Pierce, M. J. Holtzman, S. L. Brody, Myb permits multilineage airway epithelial cell differentiation. *Stem Cells* **32**, 3245–3256 (2014).
38. A. O. Yildirim, M. Veith, T. Rausch, B. Müller, P. Kilb, L. S. Van Winkle, H. Fehrenbach, Keratinocyte growth factor protects against Clara cell injury induced by naphthalene. *Eur. Respir. J.* **32**, 694–704 (2008).
39. F. J. Milder, L. Gomes, A. Schouten, B. J. C. Janssen, E. G. Huizinga, R. A. Romijn, W. Hemrika, A. Roos, M. R. Daha, P. Gros, Factor B structure provides insights into activation of the central protease of the complement system. *Nat. Struct. Mol. Biol.* **14**, 224–228 (2007).
40. C. Hess, C. Kemper, Complement-mediated regulation of metabolism and basic cellular processes. *Immunity* **45**, 240–254 (2016).
41. L. T. Roumenina, M. V. Daugan, F. Petitprez, C. Sautès-Fridman, W. H. Fridman, Context-dependent roles of complement in cancer. *Nat. Rev. Cancer* **19**, 698–715 (2019).
42. B. C. King, A. M. Blom, Complement in metabolic disease: Metaflammation and a two-edged sword. *Semin. Immunopathol.* **43**, 829–841 (2021).
43. A. Sünderhauf, K. Skibbe, S. Preisker, K. Ebbert, A. Verschoor, C. M. Karsten, C. Kemper, M. Huber-Lang, M. Basic, A. Bleich, J. Büning, K. Fellermann, C. Sina, S. Derer, Regulation of epithelial cell expressed C3 in the intestine—Relevance for the pathophysiology of inflammatory bowel disease? *Mol. Immunol.* **90**, 227–238 (2017).
44. Y. Laumonnier, C. M. Karsten, J. Köhl, Novel insights into the expression pattern of anaphylatoxin receptors in mice and men. *Mol. Immunol.* **89**, 44–58 (2017).
45. M. Elvington, M. K. Liszewski, J. P. Atkinson, Evolution of the complement system: From defense of the single cell to guardian of the intravascular space. *Immunol. Rev.* **274**, 9–15 (2016).
46. C. Homann, K. Varming, K. Høgåsen, T. E. Mollnes, N. Graudal, A. C. Thomsen, P. Garred, Acquired C3 deficiency in patients with alcoholic cirrhosis predisposes to infection and increased mortality. *Gut* **40**, 544–549 (1997).
47. D. K. Pillai, B.-J. V. Sankoorikal, E. Johnson, A. N. Seneviratne, J. Zurko, K. J. Brown, Y. Hathout, M. C. Rose, Directional secretomes reflect polarity-specific functions in an in vitro model of human bronchial epithelium. *Am. J. Respir. Cell Mol. Biol.* **50**, 292–300 (2014).
48. J. R. Peters-Hall, K. J. Brown, D. K. Pillai, A. Tomney, L. M. Garvin, X. Wu, M. C. Rose, Quantitative proteomics reveals an altered cystic fibrosis in vitro bronchial epithelial secretome. *Am. J. Respir. Cell Mol. Biol.* **53**, 22–32 (2015).
49. E. L. Rawlins, T. Okubo, Y. Xue, D. M. Brass, R. L. Auten, H. Hasegawa, F. Wang, B. L. M. Hogan, The role of Scgb1a1$^+$ Clara cells in the long-term maintenance and repair of lung airway, but not alveolar, epithelium. *Cell Stem Cell* **4**, 525–534 (2009).
50. M. K. Liszewski, M. Kolev, G. Le Friec, M. Leung, P. G. Bertram, A. F. Fara, M. Subias, M. C. Pickering, C. Drouet, S. Meri, T. P. Arstila, P. T. Pekkarinen, M. Ma, A. Cope, T. Reinheckel, S. Rodriguez de Cordoba, B. Afzali, J. P. Atkinson, C. Kemper, Intracellular complement activation sustains T cell homeostasis and mediates effector differentiation. *Immunity* **39**, 1143–1157 (2013).
51. Y. Lu, L. Parkyn, L. E. Otterbein, Y. Kureishi, K. Walsh, A. Ray, P. Ray, Activated Akt protects the lung from oxidant-induced injury and delays death of mice. *J. Exp. Med.* **193**, 545–550 (2001).
52. B. D. Manning, L. C. Cantley, AKT/PKB signaling: Navigating downstream. *Cell* **129**, 1261–1274 (2007).
53. N. Niyonzima, J. Rahman, N. Kunz, E. E. West, T. Freiwald, J. V. Desai, N. S. Merle, A. Gidon, B. Sporsheim, M. S. Lionakis, K. Evensen, B. Lindberg, K. Skagen, M. Skjelland, P. Singh, M. Haug, M. M. Ruseva, M. Kolev, J. Bibby, O. Marshall, B. O'Brien, N. Deeks, B. Afzali, R. J. Clark, T. M. Woodruff, M. Pryor, Z.-H. Yang, A. T. Remaley, T. E. Mollnes, S. M. Hewitt, B. Yan, M. Kazemian, M. G. Kiss, C. J. Binder, B. Halvorsen, T. Espevik, C. Kemper, Mitochondrial C5aR1 activity in macrophages controls IL-1β production underlying sterile inflammation. *Sci Immunol* **6**, eabf2489 (2021).
54. M. Ishii, G. Beeson, C. Beeson, B. Rohrer, Mitochondrial C3a receptor activation in oxidatively stressed epithelial cells reduces mitochondrial respiration and metabolism. *Front. Immunol.* **12**, 628062 (2021).
55. P. Atanes, I. Ruz-Maldonado, A. Pingitore, R. Hawkes, B. Liu, M. Zhao, G. C. Huang, S. J. Persaud, S. Amisten, C3aR and C5aR1 act as key regulators of human and mouse β-cell function. *Cell. Mol. Life Sci.* **75**, 715–726 (2018).
56. W. Posch, J. Vosper, A. Noureen, V. Zaderer, C. Witting, G. Bertacchi, R. Gstir, P. A. Filipek, G. K. Bonn, L. A. Huber, R. Bellmann-Weiler, C. Lass-Flörl, D. Wilflingseder, C5aR inhibition of nonimmune cells suppresses inflammation and maintains epithelial integrity in SARS-CoV-2-infected primary human airway epithelia. *J. Allergy Clin. Immunol.* **147**, 2083–2097.e6 (2021).
57. K. Heinzelmann, Q. Hu, Y. Hu, E. Dobrinskikh, M. Ansari, M. C. Melo-Narváez, H. M. Ulke, C. Leavitt, C. Mirita, T. Trudeau, M. L. Saal, P. Rice, B. Gao, W. J. Janssen, I. V. Yang, H. B. Schiller, E. K. Vladar, M. Lehmann, M. Königshoff, Single-cell RNA sequencing identifies G-protein coupled receptor 87 as a basal cell marker expressed in distal honeycomb cysts in idiopathic pulmonary fibrosis. *Eur. Respir. J.* **59**, 2102373 (2022).
58. R. Vittal, A. J. Fisher, E. L. Thompson, E. M. Cipolla, H. Gu, E. A. Mickler, A. Varre, M. Agarwal, K. K. Kim, M. R. Vasko, B. B. Moore, V. N. Lama, Overexpression of decay accelerating factor mitigates fibrotic responses to lung injury. *Am. J. Respir. Cell Mol. Biol.* **67**, 459–470 (2022).
59. J. I. Moliva, M. V. S. Rajaram, S. Sidiki, S. J. Sasindran, E. Guirado, X. J. Pan, S.-H. Wang, P. Ross, W. P. Lafuse, L. S. Schlesinger, J. Turner, J. B. Torrelles, Molecular composition of the alveolar lining fluid in the aging lung. *Age (Dordr.)* **36**, 9633 (2014).
60. K. Bielen, B. S. Jongers, S. Malhotra-Kumar, P. G. Jorens, H. Goossens, S. Kumar-Singh, Animal models of hospital-acquired pneumonia: Current practices and future perspectives. *Ann. Transl. Med.* **5**, 132 (2017).
61. Z. Zheng, Y.-N. Li, S. Jia, M. Zhu, L. Cao, M. Tao, J. Jiang, S. Zhan, Y. Chen, P.-J. Gao, W. Hu, Y. Wang, C. Shao, Y. Shi, Lung mesenchymal stromal cells influenced by Th2 cytokines mobilize neutrophils and facilitate metastasis by producing complement C3. *Nat. Commun.* **12**, 6202 (2021).
62. S. Kumar, M. G. Frid, H. Zhang, M. Li, S. Riddle, R. D. Brown, S. C. Yadav, M. K. Roy, M. E. Dzieciatkowska, A. D'Alessandro, K. C. Hansen, K. R. Stenmark, Complement-containing small extracellular vesicles from adventitial fibroblasts induce proinflammatory and metabolic reprogramming in macrophages. *JCI Insight* **6**, e148382 (2021).
63. F. Bastaert, S. Kheir, V. Saint-Criq, B. Villeret, P. M.-C. Dang, J. El-Benna, J.-C. Sirard, R. Voulhoux, J.-M. Sallenave, Pseudomonas aeruginosa LasB subverts alveolar macrophage activity by interfering with bacterial killing through downregulation of innate immune defense, reactive oxygen species generation, and complement activation. *Front. Immunol.* **9**, 1675 (2018).
64. L. Ma, S. K. Sahu, M. Cano, V. Kuppuswamy, J. Bajwa, J. McPhatter, A. Pine, M. L. Meizlish, G. Goshua, C.-H. Chang, H. Zhang, C. Price, P. Bahel, H. Rinder, T. Lei, A. Day, D. Reynolds, X. Wu, R. Schriefer, A. M. Rauseo, C. W. Goss, J. A. O'Halloran, R. M. Presti, A. H. Kim, A. E. Gelman, C. S. Dela Cruz, A. I. Lee, P. A. Mudd, H. J. Chun, J. P. Atkinson, H. S. Kulkarni, Increased complement activation is a distinctive feature of severe SARS-CoV-2 infection. *Sci. Immunol.* **6**, eabh2259 (2021).
65. T. Okamoto, S. K. Mathai, C. E. Hennessy, L. A. Hancock, A. D. Walts, A. L. Stefanski, K. K. Brown, D. A. Lynch, G. P. Cosgrove, S. D. Groshong, C. D. Cool, M. I. Schwarz, N. K. Banda, J. M. Thurman, I. V. Yang, V. M. Holers, D. A. Schwartz , The relationship between complement C3 expression and the MUC5B genotype in pulmonary fibrosis. *Am. J. Physiol. Lung Cell Mol. Physiol.* **315**, L1– L10 (2018).
66. P. S. Hair, L. A. Sass, T. Vazifedan, T. A. Shah, N. K. Krishna, K. M. Cunnion, Complement effectors, C5a and C3a, in cystic fibrosis lung fluid correlate with disease severity. *PLOS ONE* **12**, e0173257 (2017).
67. M. Matsumoto, W. Fukuda, A. Circolo, J. Goellner, J. Strauss-Schoenberger, X. Wang, S. Fujita, T. Hidvegi, D. D. Chaplin, H. R. Colten, Abrogation of the alternative complement pathway by targeted deletion of murine factor B. *Proc. Natl. Acad. Sci. U.S.A.* **94**, 8720–8725 (1997).

Downloaded from https://www.science.org at University of Massachusetts Worcester on February 08, 2023

68. S. Keshavjee, R. D. Davis, M. R. Zamora, M. de Perrot, G. A. Patterson, A randomized, placebo-controlled trial of complement inhibition in ischemia-reperfusion injury after lung transplantation in human beings. *J. Thorac. Cardiovasc. Surg.* **129**, 423–428 (2005).
69. D. C. Mastellos, B. G. P. Pires da Silva, B. A. L. Fonseca, N. P. Fonseca, M. Auxiliadora-Martins, S. Mastaglio, A. Ruggeri, M. Sironi, P. Radermacher, A. Chrysanthopoulou, P. Skendros, K. Ritis, I. Manfra, S. Iacobelli, M. Huber-Lang, B. Nilsson, D. Yancopoulou, E. S. Connolly, C. Garlanda, F. Ciceri, A. M. Risitano, R. T. Calado, J. D. Lambris, Complement C3 vs C5 inhibition in severe COVID-19: Early clinical findings reveal differential biological efficacy. *Clin. Immunol.* **220**, 108598 (2020).
70. N. P. du Sert, V. Hurst, A. Ahluwalia, S. Alam, M. T. Avey, M. Baker, W. J. Browne, A. Clark, I. C. Cuthill, U. Dirnagl, M. Emerson, P. Garner, S. T. Holgate, D. W. Howells, N. A. Karp, S. E. Lazic, K. Lidster, C. J. MacCallum, M. Macleod, E. J. Pearl, O. H. Petersen, F. Rawle, P. Reynolds, K. Rooney, E. S. Sena, S. D. Silberberg, T. Steckler, H. Würbel, The ARRIVE guidelines 2.0: Updated guidelines for reporting animal research. *J. Physiol.* **598**, 3793–3801 (2020).
71. A. Circolo, G. Garnier, W. Fukuda, X. Wang, T. Hidvegi, A. J. Szalai, D. E. Briles, J. E. Volanakis, R. A. Wetsel, H. R. Colten, Genetic disruption of the murine complement C3 promoter region generates deficient mice with extrahepatic expression of C3 mRNA. *Immunopharmacology* **42**, 135–149 (1999).
72. J. Kildsgaard, T. J. Hollmann, K. W. Matthews, K. Bian, F. Murad, R. A. Wetsel, Cutting edge: Targeted disruption of the C3a receptor gene demonstrates a novel protective anti-inflammatory role for C3a in endotoxin-shock. *J. Immunol.* **165**, 5406–5409 (2000).
73. L. Zou, Y. Feng, Y. Li, M. Zhang, C. Chen, J. Cai, Y. Gong, L. Wang, J. M. Thurman, X. Wu, J. P. Atkinson, W. Chao, Complement factor B is the downstream effector of TLRs and plays an important role in a mouse model of severe sepsis. *J. Immunol.* **191**, 5625–5635 (2013).
74. M. P. Triebwasser, X. Wu, P. Bertram, D. E. Hourcade, D. M. Nelson, J. P. Atkinson, Timing and mechanism of conceptus demise in a complement regulatory membrane protein deficient mouse. *Am. J. Reprod. Immunol.* **80**, e12997 (2018).
75. A. Heeckeren, R. Walenga, M. W. Konstan, T. Bonfield, P. B. Davis, T. Ferkol, Excessive inflammatory response of cystic fibrosis mice to bronchopulmonary infection with Pseudomonas aeruginosa. *J. Clin. Invest.* **100**, 2810–2815 (1997).
76. Details about the COMPBIO biological knowledge generation platform are available on the websites of the Washington University School Medical Library (https://becker.wustl.edu/resources/software/compbio/) and the company website for PercayAI (www.percayai.com/tech).
77. H. S. Kulkarni, J. S. Lee, J. A. Bastarache, W. M. Kuebler, G. P. Downey, G. M. Albaiceta, W. A. Altemeier, A. Artigas, J. H. T. Bates, C. S. Calfee, C. S. Dela Cruz, R. P. Dickson, J. A. Englert, J. I. Everitt, M. B. Fessler, A. E. Gelman, K. M. Gowdy, S. D. Groshong, S. Herold, R. J. Homer, J. C. Horowitz, C. C. W. Hsia, K. Kurahashi, V. E. Laubach, M. R. Looney, R. Lucas, N. S. Mangalmurti, A. M. Manicone, T. R. Martin, S. Matalon, M. A. Matthay, D. F. McAuley, S. A. McGrath-Morrow, J. P. Mizgerd, S. A. Montgomery, B. B. Moore, A. Noël, C. E. Perlman, J. P. Reilly, E. P. Schmidt, S. J. Skerrett, T. L. Suber, C. Summers, B. T. Suratt, M. Takata, R. Tuder, S. Uhlig, M. Witzenrath, R. L. Zemans, G. Matute-Bello, Update on the features and measurements of experimental acute lung injury in animals: An official American Thoracic Society workshop report. *Am. J. Respir. Cell Mol. Biol.* **66**, e1–e14 (2022).
78. A. Ehlers, W. Xie, E. Agapov, S. Brown, D. Steinberg, R. Tidwell, G. Sajol, R. Schutz, R. Weaver, H. Yu, M. Castro, L. B. Bacharier, X. Wang, M. J. Holtzman, J. A. Haspel, BMAL1 links the circadian clock to viral airway pathology and asthma phenotypes. *Mucosal Immunol.* **11**, 97–111 (2018).
79. H. Pan, G. H. Deutsch, S. E. Wert; On behalf of the Ontology Subcommittee & NHLBI Molecular Atlas of Lung Development Program Consortium, Comprehensive anatomic ontologies for lung development: A comparison of alveolar formation and maturation within mouse and human lung. *J. Biomed. Semantics* **10**, 18 (2019).
80. M. Deprez, L.-E. Zaragosi, M. Truchi, C. Becavin, S. Ruiz García, M.-J. Arguel, M. Plaisant, V. Magnone, K. Lebrigand, S. Abelanet, F. Brau, A. Paquet, D. Pe'er, C.-H. Marquette, S. Leroy, P. Barbry, A single-cell atlas of the human healthy airways. *Am. J. Respir. Crit. Care Med.* **202**, 1636–1645 (2020).
81. K. C. Goldfarbmuren, N. D. Jackson, S. P. Sajuthi, N. Dyjack, K. S. Li, C. L. Rios, E. G. Plender, M. T. Montgomery, J. L. Everman, P. E. Bratcher, E. K. Vladar, M. A. Seibold, Dissecting the cellular specificity of smoking effects and reconstructing lineages in the human airway epithelium. *Nat. Commun.* **11**, 2485 (2020).
82. P. A. Reyfman, J. M. Walter, N. Joshi, K. R. Anekalla, A. C. McQuattie-Pimentel, S. Chiu, R. Fernandez, M. Akbarpour, C.-I. Chen, Z. Ren, R. Verma, H. Abdala-Valencia, K. Nam, M. Chi, S. Han, F. J. Gonzalez-Gonzalez, S. Soberanes, S. Watanabe, K. J. N. Williams, A. S. Flozak, T. T. Nicholson, V. K. Morgan, D. R. Winter, M. Hinchcliff, C. L. Hrusch, R. D. Guzy, C. A. Bonham, A. I. Sperling, R. Bag, R. B. Hamanaka, G. M. Mutlu, A. V. Yeldandi, S. A. Marshall, A. Shilatifard, L. A. N. Amaral, H. Perlman, J. I. Sznajder, A. C. Argento, C. T. Gillespie, J. Dematte, M. Jain, B. D. Singer, K. M. Ridge, A. P. Lam, A. Bharat, S. M. Bhorade, C. J. Gottardi, G. R. S. Budinger, A. V. Misharin, Single-cell transcriptomic analysis of human lung provides insights into the pathobiology of pulmonary fibrosis. *Am. J. Respir. Crit. Care Med.* **199**, 1517–1536 (2019).
83. T. S. Adams, J. C. Schupp, S. Poli, E. A. Ayaub, N. Neumark, F. Ahangari, S. G. Chu, B. A. Raby, G. Deluliis, M. Januszyk, Q. Duan, H. A. Arnett, A. Siddiqui, G. R. Washko, R. Homer, X. Yan, I. O. Rosas, N. Kaminski, Single-cell RNA-seq reveals ectopic and aberrant lung-resident cell populations in idiopathic pulmonary fibrosis. *Sci. Adv.* **6**, eaba1983 (2020).
84. A. C. Habermann, A. J. Gutierrez, L. T. Bui, S. L. Yahn, N. I. Winters, C. L. Calvi, L. Peter, M.-I. Chung, C. J. Taylor, C. Jetter, L. Raju, J. Roberson, G. Ding, L. Wood, J. M. S. Sucre, B. W. Richmond, A. P. Serezani, W. J. McDonnell, S. B. Mallal, M. J. Bacchetta, J. E. Loyd, C. M. Shaver, L. B. Ware, R. Bremner, R. Walia, T. S. Blackwell, N. E. Banovich, J. A. Kropski, Single-cell RNA sequencing reveals profibrotic roles of distinct epithelial and mesenchymal lineages in pulmonary fibrosis. *Sci. Adv.* **6**, eaba1972 (2020).
85. S. V. Bardina, D. Michlmayr, K. W. Hoffman, C. J. Obara, J. Sum, I. F. Charo, W. Lu, A. G. Pletnev, J. K. Lim, Differential roles of chemokines CCL2 and CCL7 in monocytosis and leukocyte migration during west nile virus infection. *J. Immunol.* **195**, 4306–4318 (2015).
86. H.-M. Hsiao, R. Fernandez, S. Tanaka, W. Li, J. H. Spahn, S. Chiu, M. Akbarpour, D. Ruiz-Perez, Q. Wu, C. Turam, D. Scozzi, T. Takahashi, H. P. Luehmann, V. Puri, G. R. S. Budinger, A. S. Krupnick, A. V. Misharin, K. J. Lavine, Y. Liu, A. E. Gelman, A. Bharat, D. Kreisel, Spleen-derived classical monocytes mediate lung ischemia-reperfusion injury through IL-1β. *J. Clin. Invest.* **128**, 2833–2847 (2018).
87. Y. Cao, T. Vo, G. Millien, J.-B. Tagne, D. Kotton, R. J. Mason, M. C. Williams, M. I. Ramirez, Epigenetic mechanisms modulate thyroid transcription factor 1-mediated transcription of the surfactant protein B gene. *J. Biol. Chem.* **285**, 2152–2164 (2010).
88. Y. Zhang, S. Yokoyama, J. C. Herriges, Z. Zhang, R. E. Young, J. M. Verheyden, X. Sun, E3 ubiquitin ligase RFWD2 controls lung branching through protein-level regulation of ETV transcription factors. *Proc. Natl. Acad. Sci. U.S.A.* **113**, 7557–7562 (2016).
89. J. L. Proenca-Modena, R. Sesti-Costa, A. K. Pinto, J. M. Richner, H. M. Lazear, T. Lucas, J. L. Hyde, M. S. Diamond, Oropouche virus infection and pathogenesis are restricted by MAVS, IRF-3, IRF-7, and type I interferon signaling pathways in nonmyeloid cells. *J. Virol.* **89**, 4720–4737 (2015).
90. M. S. Kuefner, K. Pham, J. R. Redd, E. J. Stephenson, I. Harvey, X. Deng, D. Bridges, E. Boilard, M. B. Elam, E. A. Park, Secretory phospholipase A2 group IIA modulates insulin sensitivity and metabolism. *J. Lipid Res.* **58**, 1822–1833 (2017).

Acknowledgments: We thank C. Kemper, D. Hourcade, J. Haspel, M. Holtzman, J. Koenitzer, and Y.-C. Perng for insights on the work and contribution of reagents. We thank L. Mitchell, K. Liszewski, C. Gierasch, J. Xu, J.-H. Pan, S. Gunsten, T. Huang, C. Min, and A. Pesavento for technical assistance. **Funding:** This research was financed by the National Heart, Lung, and Blood Institute of the NIH (grant K08HL148510 to H.S.K.); National Institute of General Medical Sciences of the NIH (grant R35GM136352 to J.P.A.); National Eye Institute of the NIH (grant R01EYE028602 to J.P.A.); Children's Discovery Institute (to H.S.K.); Rheumatic Diseases Research Resource-Based Center (project number P30AR073752 to H.S.K.); the Clark Family/Clayco Foundation International Cerebroretinal Vasculopathy (CRV) Research Award (to J.P.A.); and the Foundation for Barnes-Jewish Hospital (to S.L.B.). Experimental support was also partially provided by the Bursky Center for Human Immunology and Immunotherapy Programs at Washington University Immunomonitoring Laboratory, in support of the Rheumatic Diseases Core Center (project number NIH WLC6313040077). **Author contributions:** Conceptualization: H.S.K., S.L.B., and J.P.A. Methodology: A.N.O., D.H.K., S.K.S., L.D., M.S., L.M., J.M., L.G., J.K., and X.W. Investigation: H.S.K., A.N.O., D.H.K., L.D., A.L., M.S., and S.K.S. Visualization: H.S.K., A.N.O., D.H.K., L.D., M.S., R.A.B., and S.K.S. Funding acquisition: H.S.K. and J.P.A. Project administration: H.S.K. Supervision: H.S.K. and J.P.A. Writing (original draft): H.S.K., A.N.O., S.K.S., R.A.B., J.P.A., and S.L.B. Writing (review and editing): H.S.K., A.N.O., D.H.K., R.A.B., S.K.S., L.D., A.L., M.S., M.S.-B., L.M., J.M., L.G., J.K., X.W., A.E.G., J.P.A., and S.L.B. **Competing interests:** H.S.K. reports receiving grant funding for Alexion Pharmaceuticals unrelated to the submitted work. H.S.K. reports serving as a paid consultant for Guidepoint Global Advisors and Arrowhead Pharmaceuticals. J.P.A. reports serving as a consultant for Celldex Therapeutics, Clinical Pharmacy Services, Kypha Inc., Achillion Pharmaceuticals Inc., and BioMarin Pharmaceutical Inc. J.P.A. has stock or equity options in Compliment Corporation, Kypha Inc., Gemini Therapeutics, and Q32 Bio. S.L.B. has received laboratory research funds from Genentech. R.A.B. may receive royalty income based on the COMPBIO method developed by R.A.B. and licensed by Washington University to PercayAI. The other authors declare that they have no competing interests. **Data and materials availability:** The RNA-seq dataset has been deposited on NCBI GEO [www.ncbi.nlm.nih.gov/geo/ (GSE218554)]. All other data needed to evaluate the reported conclusions are present in the paper or the Supplementary Materials.

Submitted 8 March 2022
Resubmitted 27 November 2022
Accepted 11 January 2023
Published 3 February 2023
10.1126/sciimmunol.abp9547

Downloaded from https://www.science.org at University of Massachusetts Worcester on February 08, 2023

Science Immunology

Lung epithelial cell–derived C3 protects against pneumonia-induced lung injury

Sanjaya K. Sahu, Aye N. Ozantrk, Devesha H. Kulkarni, Lina Ma, Ruteja A. Barve, Linus Dannull, Angel Lu, Marick Starick, JaNia McPhatter, Lorena Garnica, Maxwell Sanfillipo-Burchman, Jeremy Kunen, Xiaobo Wu, Andrew E. Gelman, Steven L. Brody, John P. Atkinson, and Hrishikesh S. Kulkarni

Sci. Immunol., **8** (80), eabp9547.
DOI: 10.1126/sciimmunol.abp9547

Lung protection by local complement

Complement proteins are innate immune defense molecules that protect the host against pathogenic microorganisms. The activities of the C3 component of complement are mostly attributed to circulating C3 primarily synthesized by hepatocytes. Sahu and Ozantürk *et al*. used mouse models of conditional gene deletion to investigate the contribution of local C3 protein production in the lung to protecting the pulmonary mucosal surface from cell damage caused by *Pseudomonas aeruginosa* infection. Mice lacking C3 only in lung epithelial cells exhibited more pronounced acute lung injury than control mice even so circulating C3 levels were maintained at near-normal levels by maintenance of liver C3 production. These findings point to lung epithelial cell-intrinsic protective functions provided by C3 as an essential contributor to first-line defense against bacterial pneumonia.—IRW

View the article online
https://www.science.org/doi/10.1126/sciimmunol.abp9547
Permissions
https://www.science.org/help/reprints-and-permissions

Downloaded from https://www.science.org at University of Massachusetts Worcester on February 08, 2023

Use of this article is subject to the Terms of service

Science Immunology (ISSN) is published by the American Association for the Advancement of Science. 1200 New York Avenue NW, Washington, DC 20005. The title *Science Immunology* is a registered trademark of AAAS.
Copyright © 2023 The Authors, some rights reserved; exclusive licensee American Association for the Advancement of Science. No claim to original U.S. Government Works